AD-A230 614

ENERGY TRANSFER IN
SINGLET OXYGEN AND
BROMINE MONOFLUORIDE

THESIS

Barrett F. Lowe
Captain, US Army

AFIT/GEP/ENP/90D-2

DEPARTMENT OF THE AIR FORCE

AIR UNIVERSITY

AIR FORCE INSTITUTE OF TECHNOLOGY

Wright-Patterson Air Force Base, Ohio

91 1 3 108

AFIT/GEP/ENP/90D-2

DTIC
ELECTE.
JAN 07 1991
S   D
D

ENERGY TRANSFER IN
SINGLET OXYGEN AND
BROMINE MONOFLUORIDE

THESIS

Barrett F. Lowe
Captain, US Army

AFIT/GEP/ENP/90D-2

AFIT/GEP/ENP/90D-2

ENERGY TRANSFER IN
SINGLET OXYGEN AND
BROMINE MONOFLUORIDE

THESIS

Presented to the Faculty of the School of Engineering

of the Air Force Institute of Technology

Air University

In Partial Fulfillment of the

Requirements for the Degree of

Master of Science in Engineering Physics

Barrett F. Lowe, B.S.

Captain, US Army

December, 1990

Preface

This research was part of the continuing study to characterize the energy transfer between singlet oxygen and interhalogen molecules in determining potential candidates for a visible chemical laser system. The primary goal of this research was to use chemiluminescence experiments to determine the mechanism by which $O_2(^1\Sigma)$ pumps BrF(B). Supplementary goals of determining rate constants, efficiency, and the vibrational distribution of the BrF(B) state were also completed.

I found the research to be an extremely rewarding and challenging experience. The knowledge and experience I gained in this detailed experimental research was an integral part of my AFIT studies. I am profoundly grateful to my advisor, Capt. Glen P. Perram, for his guidance, instruction, advice, and encouragement in the conduct of this research. His generous expenditure of time and effort is also acknowledged. I am equally indebted to Capt. David W. Melton, a doctoral candidate, for his assistance and comradeship in all phases of this project. I think the three of us made a great research team. I would also like to thank Mr. Greg Smith and Mr. Bill Evans for their support with the test equipment, and keeping the project supplied with the reactant gases needed for the experiments. I am also appreciative of Mr. Jimmy Ray for making the many glass elements used in the experiments, as well as repairing them on short notice.

I also wish to thank my classmates of Section GEP-90D for their friendship throughout the program and in helping me maintain my sense of humor.

Finally, I wish to sincerely thank my wife, Betsy, for her support through the 18 months of the program. Without her love, understanding, and patience in taking care of the home front, I could not have devoted the time necessary to complete this project.

Barrett F. Lowe

Table of Contents

List of Figures

List of Tables

AFIT/GEP/ENP/90D-2

Abstract

The interhalogen molecule, bromine monofluoride (BrF), is currently under study as a potential candidate for a visible chemical laser medium. Previous studies have shown a strong emission from $BrF(B^3\Pi(O_u^+))$ in the presence of singlet oxygen, $O_2(^1\Sigma)$ and $O_2(^1\Delta)$. While singlet oxygen will pump BrF(X) to BrF(B), the exact mechanism is not known. Chemiluminescence observed from BrF(B) excited by oxygen, $O_2(^1\Sigma)$ in a gas flowtube was used to study the energy transfer mechanism. The objective of this research was fourfold. First, the pumping process was identified as a 3-Body Mechanism. Second, the observed vibrational distribution clearly showed the population of the BrF(B) state to be non-Maxwellian. Third, the quenching rates for CO_2 and CF_4 on $O_2(^1\Sigma)$ were experimentally verified with the literature values, and the quenching rates for Br and Br_2 on $O_2(^1\Sigma)$ are reported for the first time. And fourth, the efficiency of the system is shown to be low, on the order of 10^{-4}.

ENERGY TRANSFER IN
SINGLET OXYGEN AND
BROMINE MONOFLUORIDE

I. Introduction

1.1 Motivation

The Air Force and the Strategic Defense Initiative Organization (SDIO) are interested in developing a new class of laser operating in the visible region under chemical excitation for directed energy weapons as well as for imaging and diagnostics applications. Chemically pumped, electronic transition lasers are particularly suited for these missions because they require no massive external power supply (the chemical reaction is a self-contained energy source), and laser output in the the visible region reduces the beam divergence, provides better atmospheric transmission. and inherently more power delivered to the target(1). While no visible chemical lasers have been produced yet, one potentially viable excitation scheme is to use the energy transferred from a metastable excited molecule to a suitable laser species. The diatomic interhalogens are a promising class of molecules that have the potential for lasing at short wavelengths (from 0.2μm to 1.3μm) after excitation by singlet oxygen(2). Many spectroscopic and kinetic studies of iodine monofluoride (IF) have been conducted and an optically pumped IF(B-X) laser has been demonstrated(3). However, studies of bromine monofluoride (BrF) have only recently been started in an attempt to assess its potential as a visible chemical laser(4).

As part of the overall project to characterize the collisional dynamics of excited BrF at AFIT(4), this research will focus on the study of the energy transfer from

metastable excited O_2 (singlet oxygen) to BrF; somewhat in analogy with using singlet oxygen in the Chemical Oxygen-Iodine Laser (COIL)(1). Previous studies have uncovered a strong visible emission from BrF in the presence of singlet $O_2(5)$, but the excitation mechanism(s), reaction rate(s), and efficiency of the excitiation process(es) have not been characterized. This research will use a standard kinetic flow tube study(6) in an attempt to characterize the excitation of BrF($B^3\Pi$) by $O_2(b^1\Sigma, a^1\Delta)$.

1.2 Problem Statement

The exact mechanism with which singlet O_2 excites BrF(X → B) has not been completely defined. BrF(X) requires at least 18272 cm^{-1} of energy to be pumped to BrF(B)(v" = 0 → to v' = 0) (4, 12). A single molecule of singlet O_2 does not have sufficient energy to excite BrF(X) directly to BrF(B). The energies of the two singlet O_2 states are 7882 cm^{-1} for $O_2(^1\Delta)$ and 13121 cm^{-1} for $O_2(^1\Sigma)$, for (v' = 0 to v" = 0) transitions respectively (18). Clearly then, some multiple collision excitation process is indicated. Clyne, Coxon, and Townsend (5) postulate a three-body excitation mechanism:

$$Br + F + M \longrightarrow BrF^* + M$$
$$BrF^* + O_2(^1\Sigma, ^1\Delta) \longrightarrow BrF(B) + O_2(^3\Sigma)$$
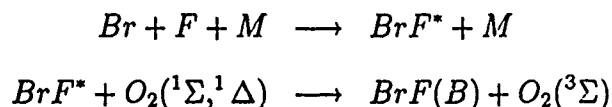
where BrF* is some excited intermediate state, and M is a third-body. This reaction will be designated the 3-Body Reaction. Another possibility is:

$$F + Br_2 \longrightarrow BrF(X) + Br$$
$$BrF(X) + O_2(^1\Sigma, ^1\Delta) \longrightarrow BrF^* + O_2(^3\Sigma)$$

2

$$BrF^* + O_2(^1\Delta, {}^1\Sigma) \longrightarrow BrF(B) + O_2(^3\Sigma)$$
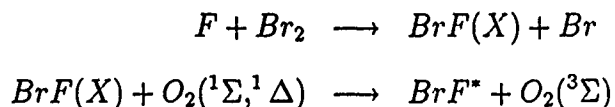
where BrF* is some excited intermediate state. This reaction will be designated the 2-Step Reaction.

This research will begin with the production of BrF molecules in the flow tube apparatus designed by Melton(4), and then creating BrF(B) molecules through collisional energy transfer with singlet O_2. The first part of the experiment will be to record the chemiluminescence spectra of the BrF in the presence of singlet O_2. The second part of the experiment will be to determine the excitation mechanism for BrF(B). These measurements are necessary in order to continue examining the collisional dynamics of excited state BrF. The next part of the research will focus on analyzing the resulting data to determine the reaction rate(s), and efficiency of this chemical process, as well as gain some insight into the vibrational populations of BrF(B) as excited by singlet O_2. The last part of this resarch will be a comparison of the BrF results with other interhalogens to determine BrF's relative suitability as a potential candidate for a visible chemical laser.

II. Background Theory

2.1 Important Laser Characteristics

This section will highlight the important characteristics the BrF molecule displays for laser operation that have been determined in spectroscopic and kinetic studies. Specifically, the ease in obtaining a population inversion in the BrF molecule, its relatively long radiative lifetime, and quenching rate information will be discussed.

Davis reports in his review on the potential for halogen molecules in visible chemical laser systems that the primary reason these molecules have a high potential for use in laser applications is the large shift of the equilibrium internuclear separation of the $B^3\Pi(0^+)$ state with respect to the $X^1\Sigma^+$ state(7). This situation is graphically portrayed in Figure 1. Therefore, according to the Franck-Condon principle, the most probable downward $B \longrightarrow X$ transitions will terminate on high vibrational levels of the ground state(7). Furthermore, in a thermal distribution at room temperature these upper vibrational levels will essentially be empty; and in BrF with a fractional population of the lower laser level of v" = 8 of $2.2x10^{-12}$ (most probable v' - v" transition from 0 - 8 using Franck-Condon factors)(7). This is characteristic of a Boltzmann population distribution @ 300 K. This means it should be easy to obtain a population inversion between a B-state v' level and an X-state v" level because with the v" level initially unpopulated, the total B-state population will not have to exceed the X-state population (7).

The collision-free lifetimes (radiative and pre-dissociative combined) of some of the B-state v' levels showing metastable characteristics, i. e. lifetimes on the order of tens of μsec, are shown in Table 1 (7, 8). A relatively long radiative lifetime is important in maintaining a population inversion in a continuous wave (cw) laser. However, Davis also indicates a repulsive state near the upper v' levels of the B-state that introduces a phenomenon called predissociation, that essentially

4
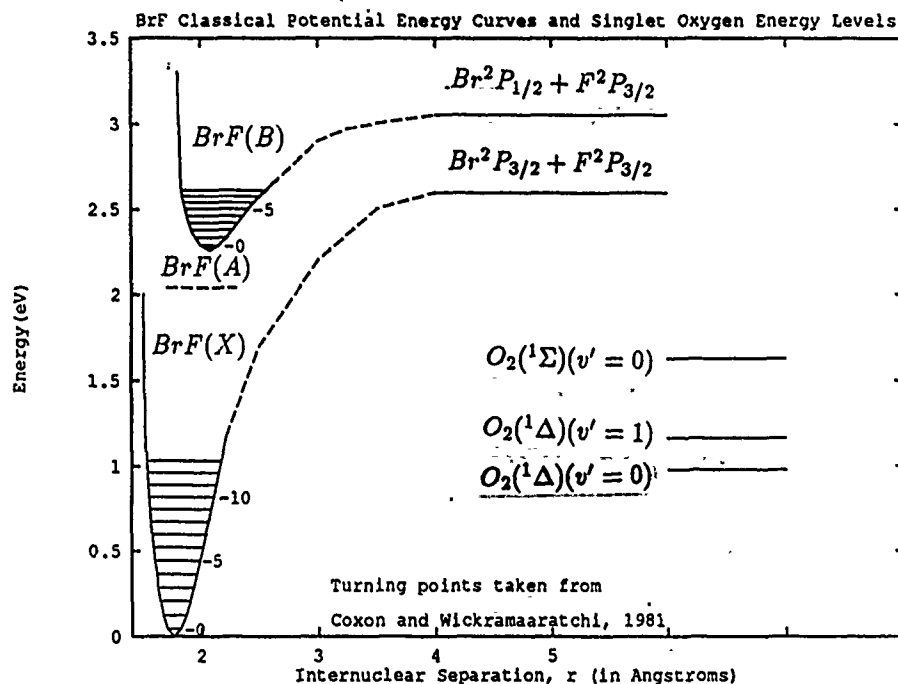
Figure 1. Potential Energy Curves for BrF(X) and BrF(B)

makes the B-state unstable(7). In BrF, Melton shows that predissociation is where the ov·rlap of the $B^3\Pi(0^+)$ state with the Y-state can allow a transition from an excited molecular state to separate atoms(4). This causes a problem by shortening the collisionless lifetime of the B-state and depletes the excited population by a nonradiative process(7). Davis emphasizes that the important characteristic to be noted is that the v' levels from 0 to 6 are metastable and the onset of predissociation is sharp at v' = 7, j' = 29(7). A higher intensity of emission due to the v' = 0 to 6 will be noted than for v' = 7 and 8. This effect can also be seen in Table 1 from Steinfeld which shows the lifetimes decrease as the v' level increases(4, 12).

2.2 Current BrF Spectroscopic Data

The current information about the BrF molecule obtained from spectroscopic studies is quite complete, especially in the areas of absorption(9) and emission(5, 10).

Table 1. BrF (B $\longrightarrow$ X) Collision Free Lifetimes (12)

V'	J'	$\tau_r(\mu sec)$	Est. Error
0	16-26	43.0	1-2%
1	5-31	44.0	1-2%
2	7-39	46.0	1-2%
3	9-42	43.9	1-2%
4	3-45	44.7	1-2%
5	3-38	44.2	1-2%
6	3-44	46.3	1-2%
6	45	62.1	$\leq$5%
6	46	58.8	$\leq$5%
6	47	50.3	$\leq$5%
6	48	10.4	$\leq$5%
7	3-26	48.1	1-2%
7	27	60.1	$\leq$5%
7	28	59.4	$\leq$5%
7	29	1.6	10%
7	30	1.16	10%
7	31	0.74	10%
8	2-27	0.3-1.7	1-2%
8	28	0.24	10%
8	29	0.14	10%
8	30	0.17	10%
8	31	0.11	10%

where $\frac{1}{\tau} = \frac{1}{\tau_r} + \frac{1}{\tau_{pd}}$

$\tau \equiv$ collision free lifetime

$\tau_r \equiv$ radiative lifetime

$\tau_{pd} \equiv$ pre-dissociative lifetime

Melton has tabulated this(4) and the spectroscopic constants for BrF are included as Table 2(12). The potential curves for BrF have previously been illustrated at Figure 1. Melton also records the Franck-Condon factors for BrF(4, 11) and these are listed in Table 3. The radiative lifetimes of the B-state v' levels are shown in Table 1(4, 12).

Table 2. Molecular Constants for BrF (in cm^{-1}) (12)

Constant	BrF(X)	BrF(B)
T_e	0	18272
D_e	20953	6366
ω_e	670.75	372.2
$\omega_e x_e$	4.054	3.49
$\omega_e y_e$	-8.7x10^{-3}	-0.22
β_e	0.35584	0.264
α_e	0.00261	0.00498
γ_e	1.06x10^{-5}	unknown
D_v	0.4x10^{-6}	1.0x10^{-6}

The dotted line depicting the location of the potential minimum for BrF(A) on the potential energy curve (Figure 1, etc.) was taken from Brodersen and Sicre's work (21). Thus far, this work is the only case where a BrF(A→X) energy system is reported. Coxon disagrees with Brodersen and Sicre claiming that the absorption data they report supporting the existence of BrF(A) is compatible only with a dissociation energy much larger than derived in their work (22). The plots in this work showing potential energy curves for BrF will use this reported location for BrF(A) as a place to illustrate the unknown excited intermediate state of BrF. This state could in fact be BrF(A), or possibly, BrF(X)(v>> 0) at a location lower than depicted.

2.3 Current Singlet Oxygen Data

The term singlet oxygen refers to the first two electronic states of diatomic molecular oxygen. A summary of pertinent information is given in Table 4.

Table 3. Franck-Condon Factors for BrF (11)

V' V"	0	1	2	3	4	5	6	7	8
0	.0000	.0002	.0006	.0016	.0033	.0060	.0096	.0140	.0179
1	.0004	.0021	.0060	.0126	.0214	.0315	.0410	.0483	.0499
2	.0026	.0109	.0250	.0418	.0556	.0623	.0600	.0501	.0347
3	.0103	.0345	.0600	.0738	.0682	.0489	.0256	.0079	.0004
4	.0296	.0726	.0875	.0671	.0310	.0056	.0005	.0101	.0211
5	.0635	.1044	.0723	.0205	.0000	.0126	.0313	.0360	.0251
6	.1073	.1012	.0235	.0014	.0288	.0453	.0319	.0099	.0001
7	.1480	.0589	.0004	.0392	.0526	.0222	.0006	.0075	.0213
8	.1657	.0113	.0334	.0625	.0180	.0011	.0234	.0347	.0207
9	.1541	.0030	.0737	.0274	.0026	.0355	.0368	.0101	.0002
10	.1263	.0418	.0661	.0000	.0410	.0389	.0036	.0074	.0250
11	.0899	.0966	.0216	.0311	.0512	.0030	.0163	.0366	.0182
12	.0526	.1244	.0003	.0678	.0117	.0166	.0427	.0129	.0010
13	.0271	.1196	.0304	.0518	.0051	.0488	.0137	.0046	.0274

Table 4. Singlet Oxygen Data

Species	Energy (cm^{-1})	Energy (eV)	Lifetime (τ_r)
$O_2(b^1\Sigma)(v'=0)$	13121	1.627	12 sec
$O_2(a^1\Delta)(v'=1)$	9367	1.1614	
$O_2(a^1\Delta)(v'=0)$	7882	0.977	65 min

As discussed previously, energy transfer from one of either of the two singlet oxygen molecules will not provide sufficient energy to pump BrF(X) to BrF(B). However, energy transfer from multiple collisions could provide enough energy for this excitation.

Extensive work done by Mack at AFIT (20) indicates singlet oxygen production in a microwave discharge at 2.45 Ghz will produce $\sim 5-15\%$ $O_2(^1\Delta)$ and $\sim 0.5-1.5\%$ $O_2(^1\Sigma)$. An average value of 10% and 1% respectively will be used in the following rate equations. With a stable flow pressure of ground state O_2 (abbreviated $O_2(x)$) of ≈ 3 torr, then the concentration of of $O_2(x)$ entering the microwave cavity is $[O_2(x)]$

8

$\approx 1.0 \times 10^{17} molecules\ cm^{-3}$. This then results in a concentration of $O_2(a)$ of $[O_2(a)]$ $\approx 1.0 \times 10^{16} molecules\ cm^{-3}$. The small amount of $O_2(b)$ produced in the microwave will be neglected due to its short radiative lifetime, a reasonable assumption that it will be quenched by wall effects and $O_2(x)$ by the time it reaches the flow tube, and that the $O_2(a)$ pooling reaction will dominate the production of $O_2(b)$ in the flow tube. Given these conditions, the rate equations for the production of $O_2(b)$ are:

$$[O_2(a)] + [O_2(a)] \xrightarrow{k_{pool}} [O_2(b)] + [O_2(x)] \tag{1}$$

$$[O_2(b)] \xrightarrow{k_{wall}} [O_2(x)] \tag{2}$$

$$[O_2(b)] \xrightarrow{1/\tau_r} [O_2(x)] + h\nu \tag{3}$$

where:

$\tau_r = 12 sec$ (18)

$k_{pool} = 2.0 \times 10^{-17} cm^3 molecule^{-1} sec^{-1}$ (18)

$k_{wall} \approx 50 sec^{-1}$ includes effects of the walls, $O_2(x)$, and impurities in the gas (determined experimentally); in effect the pseudo-first order rate coefficient.

Then in steady-state, where $d[O_2(b)]/dt = 0$, the concentration of $O_2(b)$ will be:

$$[O_2(b)] = \frac{[O_2(a)]^2 k_{pool}}{(k_{wall} + 1/\tau_r)} \tag{4}$$

$$[O_2(b)] \approx 4.0 \times 10^{13} molecules\ cm^{-3} \tag{5}$$

And this steady-state distribution shows the ratios of the concentration of the oxygen species to be $\frac{[O_2(b)]}{[O_2(x)]}$ is on the order of 10^{-4} and $\frac{[O_2(b)]}{[O_2(a)]}$ is on the order of 10^{-3}, which is in agreement with Mack's work (20).

Characterization work conducted by Melton prior to beginning the chemilumi-nescence experiments on BrF verified the quenching rate of CO_2 and CF_4 on $O_2(b)$ (26). Melton recorded a quenching rate constant for CO_2 as

$k_{qCO_2} = 3.0 \pm 0.3 x 10^{-13}$ cm^3/sec and a quenching rate constant for CF_4 as

$k_{qCF_4} = 2.68 \pm 0.3 x 10^{-15}$ cm^3/sec. These results were comparable to those recorded in previous work by Ranby and Ranek (16) and Davidson and Ogryzlo (17). A summary of these previously determined quenching rate constants is listed in Table 5.

Table 5. Recorded Quenching Rate Constants on $O_2(^1\Sigma)$

Name	Quenching Species	Constant	Value (cm^3/sec)
Davidson and Ogryzlo (17)	CO_2	$k_q(^1\Sigma)$	$3.32 x 10^{-13}$
	CO_2	$k_q(^1\Delta)$	$1.66 x 10^{-19}$
	CF_4	$k_q(^1\Sigma)$	$2.66 x 10^{-15}$
Ranby and Ranek (16)	CO_2	$k_q(^1\Sigma)$	$3.3 x 10^{-13}$
	CO_2	$k_q(^1\Delta)$	$0.5 x 10^{-18}$
Melton	CO_2	$k_q(^1\Sigma)$	$3.0 \pm 0.3 x 10^{-13}$
	CF_4	$k_q(^1\Sigma)$	$2.68 \pm 0.3 x 10^{-15}$

2.4 Reaction Mechanisms

Two primary mechanisms are hypothesized to be responsible for the excitation of BrF(B)(5, 13). The first mechanism will be called the 3-Body Mechanism, and there are two variants that will examined. Mechanism 1A will include an excited intermediate state of BrF, and Mechanism 1B will include electronically excited Br atoms as an energy carrier. The second mechanism will be called the 2-Step Mechanism and labelled as Mechanism 2. The reaction equations for these processes will be illustrated below.

First, the 3-Body Mechanism, Mechanism 1A:

$$O + Br_2 \longrightarrow BrO + Br \qquad (6)$$

10

$$O + BrO \longrightarrow Br + O_2 \tag{7}$$

$$Br + F + M \longrightarrow BrF^* + M \tag{8}$$

$$BrF^* + O_2(^1\Sigma,^1\Delta) \longrightarrow BrF(B) + O_2(^3\Sigma) \tag{9}$$
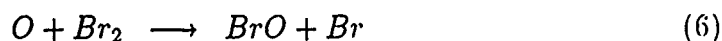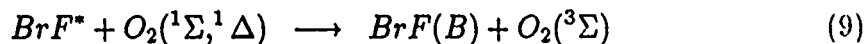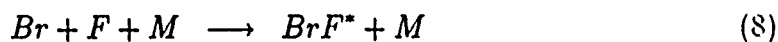
(where M is a third body and BrF^* is an excited intermediate state, either $BrF(A)$ or a high vibrational level of $BrF(X)$)

Second, the 3-Body Mechanism, Mechanism 1B:

$$O + Br_2 \longrightarrow BrO + Br \tag{10}$$

$$O + BrO \longrightarrow Br + O_2 \tag{11}$$

$$Br + O_2(^1\Sigma,^1\Delta) \longrightarrow Br^* + O_2(^1\Delta) \tag{12}$$

$$Br^* + F + M \longrightarrow BrF(B) + M \tag{13}$$
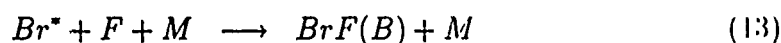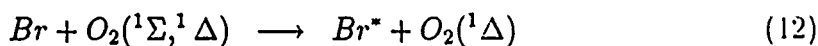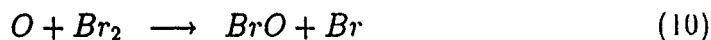
(where M is a third body and Br^* is the first electronic excited state, $Br^2P_{1/2}$)

And third, the 2-Step Mechanism, Mechanism 2:

$$F + Br_2 \longrightarrow BrF + Br \tag{14}$$

$$BrF(X) + O_2(^1\Sigma,^1\Delta) \longrightarrow BrF^* + O_2(^3\Sigma) \tag{15}$$

$$BrF^* + O_2(^\Delta,^1\Sigma) \longrightarrow BrF(B) + O_2(^3\Sigma) \tag{16}$$
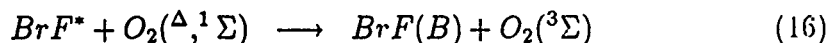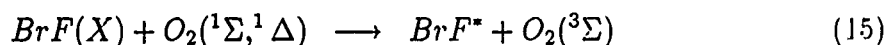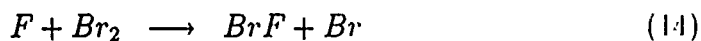
(where BrF^* is an excited intermediate state, perhaps $BrF(A)$ or a high vibrational level of BrF(X))

NOTE: For a detailed development of these rate equations, see Appendix A, Rate Equations in the Presence of Atomic Oxygen, and Appendix B, Rate Equations with CO_2 as a Quenching Species.

11

The potential energy curves on the following pages more clearly illustrate the possible mechanisms described in this section. As an additional note, to add probability to the process described in Mechanism 1B, the energy difference between the downward transition from $O_2(^1\Sigma)(v' = 0)$ to $O_2(^1\Delta)(v' = 1)$ of 3754 cm^{-1} (16, 18) and the upward transition from $Br^2P_{3/2}$ to $Br^2P_{1/2}$ of 3685 cm^{-1} (23) is only 69 cm^{-1}.

Mechanism 1A: 3-Body Mechanism

BrF Classical Potential Energy Curves and Singlet Oxygen Energy Levels
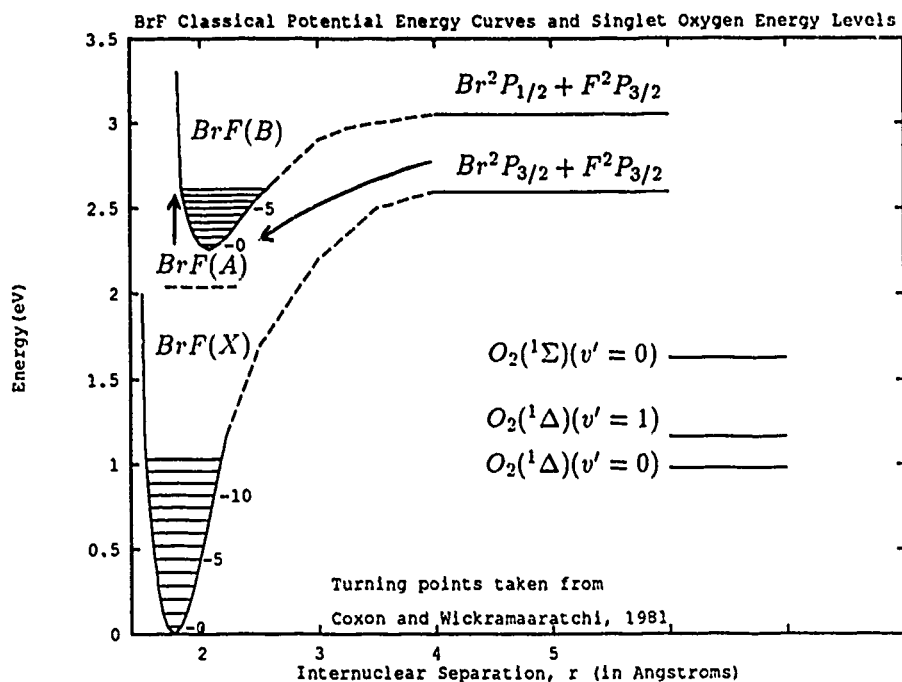
Figure 2. Mechanism 1A with Excited Intermediate State of BrF

Rate Equations:

$$Br_2 + O \longrightarrow BrO + Br^2P_{3/2}$$

$$BrO + O \longrightarrow Br^2P_{3/2} + O_2$$

$$Br^2P_{3/2} + F^2P_{3/2} + M \longrightarrow BrF^* + M$$

$$BrF^* + O_2(^1\Sigma, ^1\Delta) \longrightarrow BrF(B) + O_2(^3\Sigma)$$
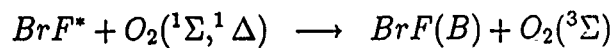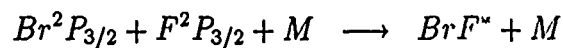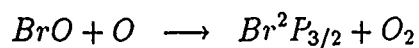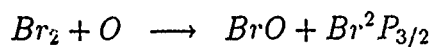
(M is mostly $O_2(^3\Sigma)$)

Mechanism 1B: 3-Body Mechanism

Figure 3. Mechanism 1B with Electronically Excited State of Br

Rate Equations:

$$Br_2 + O \longrightarrow BrO + Br^2P_{3/2}$$

$$BrO + O \longrightarrow Br^2P_{3/2} + O_2$$

$$Br^2P_{3/2} + O_2(^1\Sigma) \longrightarrow Br^2P_{1/2} + O_2(^1\Delta)$$

$$Br^2P_{1/2} + F^2P_{3/2} + M \longrightarrow BrF(B) + M$$

(M is mostly $O_2(^3\Sigma)$)

14

Mechanism 2: 2-Step Mechanism

BrF Classical Potential Energy Curves and Singlet Oxygen Energy Levels
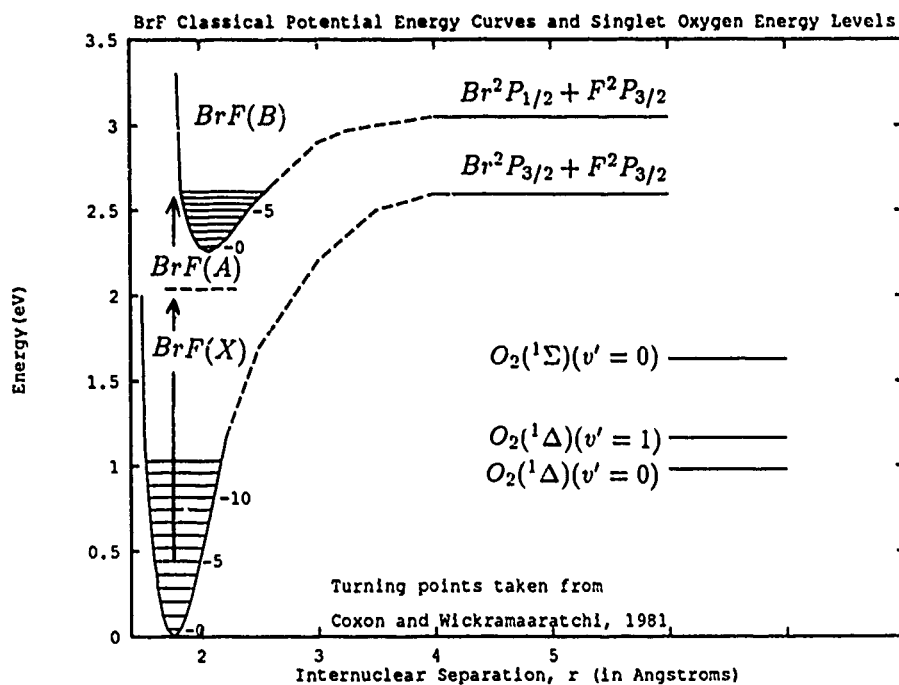
Figure 4. Mechanism 2 with Sequential Excitation

Rate Equations:

$$F + Br_2 \longrightarrow BrF(X) + Br$$

$$BrF(X) + O_2(^1\Sigma, ^1\Delta) \longrightarrow BrF^* + O_2(^3\Sigma)$$

$$BrF^* + O_2(^1\Delta, ^1\Sigma) \longrightarrow BrF(B) + O_2(^3\Sigma)$$
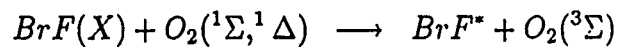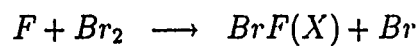
III. Description of Experiment

3.1 Production of BrF(B)

The chemiluminescence studies were conducted with the system shown in Figure 5. This apparatus was a slow-flow system with a gas velocity in the actual flow tube on the order of 1 m/sec. Three primary side-arms were used, two of which were fitted with Opthos microwave discharge cavities operating at 2.45 GHz (the O_2 inlet and the CF_4 inlet). The Br_2 inlet was inserted down the center of the flow tube to allow mixing with the O_2(b) before encountering the flow from the Cl inlet. The constituent gases were mixed directly in front of the observation windows at a total pressure of 3.4 − 3.6 $torr$. The gas products were then exhausted through a cold trap at 77 K and the Br_2 and other reagents collected for disposal.

With the flow tube apparatus as configured in Figure 5, BrF(B) was consistently produced and the yellowish glow as reported by Clyne, et al., was clearly seen(5). However, considerable difficulty was encountered in acheiving BrF(B) production at first. In the previous work, scant details on constituent gas concentrations were given. After much trial and error, the following mix produced the maximum BrF(B) signal with the described experimental set-up:

Table 6. Relative Gas Mixes for Optimum BrF(B) Production

Constituent Gas	Partial Pressure	Flow Rate	Purity (%)
O_2 (Airco)	2.9-3.0 torr	850 sccm	99.9
CF_4 (Matheson)	0.5-0.6 torr	190 sccm	99.7
Br_2 (Spectrum Chemical)	∼ 0.0006 torr	0.19 sccm	99.5

The O_2 flow was controlled using a Sierra Instruments mass flow controller. At 850 sccm, the O_2 concentration was determined to be approximately $1.0 \times 10^{17} \frac{molecules}{cm^3}$. The microwave discharge on the O_2 inlet produced both metastable O_2(a) and O_2(b) ($^1\Delta_g$ and $^1\Sigma_g^+$) as well as O atoms. A TEFLON insert was used in the flow tube itself to reduce the quenching rate due to the walls.

While BrF(B) was being produced, a measurement of the strength of the $O_2(b)$ emission as the O_2 flow was varied was conducted. The relative intensity of the emission of $O_2(b)$ at 7620 A (the center of the $O_2(b)(v' = 0 \longrightarrow v'' = 0)$ emission band) decreased as the flow was decreased or increased from 850 sccm according to the following:

O_2 Flow (sccm)	600	650	700	750	800	850	900	950
Relative Intensity(%)	56	66	74	84	92	100	100	92

The Br_2 and CF_4 flows were controlled using Nupro metering valves that had been reset to reflect no flow at the "0" setting on the dial. The Br_2 pressure was extremely small in relation to the CF_4 and O_2 pressures used. At 0°C, Br_2 has a vapor pressure of approximately 65 *torr*, and hence moves very slowly through the $\frac{1}{4}$ inch diameter metal tubing to the flow tube (the Br_2 reservoir was placed in an ice water bath to maintain a constant temperature and vapor pressure). The Br_2 concentration based on the valve calibration (Appendix C) is on the order of $2.0 \times 10^{13} \frac{molecules}{cm^3}$. Upon mixing with the microwaved O_2 flow, Br atoms were produced according to the fast reaction:

$$O + Br_2 \longrightarrow BrO + Br \qquad (17)$$

$$O + BrO \longrightarrow O_2 + Br \qquad (18)$$
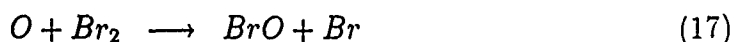
The CF_4 was dissociated in the second microwave cavity to produce ground state F atoms. CF_4 was used as the source of Fluorine atoms due to its availability, low cost, and low toxicity. Kolb and Kaufman report producing F atoms by flowing CF_4 through a microwave cavity under similar conditions with concentrations of $2.4 - 6.0 \times 10^{14} \frac{molecules}{cm^3}$, and efficiencies ranging from 1.9 - 4.7 % (27). Their studies showed only undissociated CF_4, C_2F_6, and atomic and molecular Fluorine
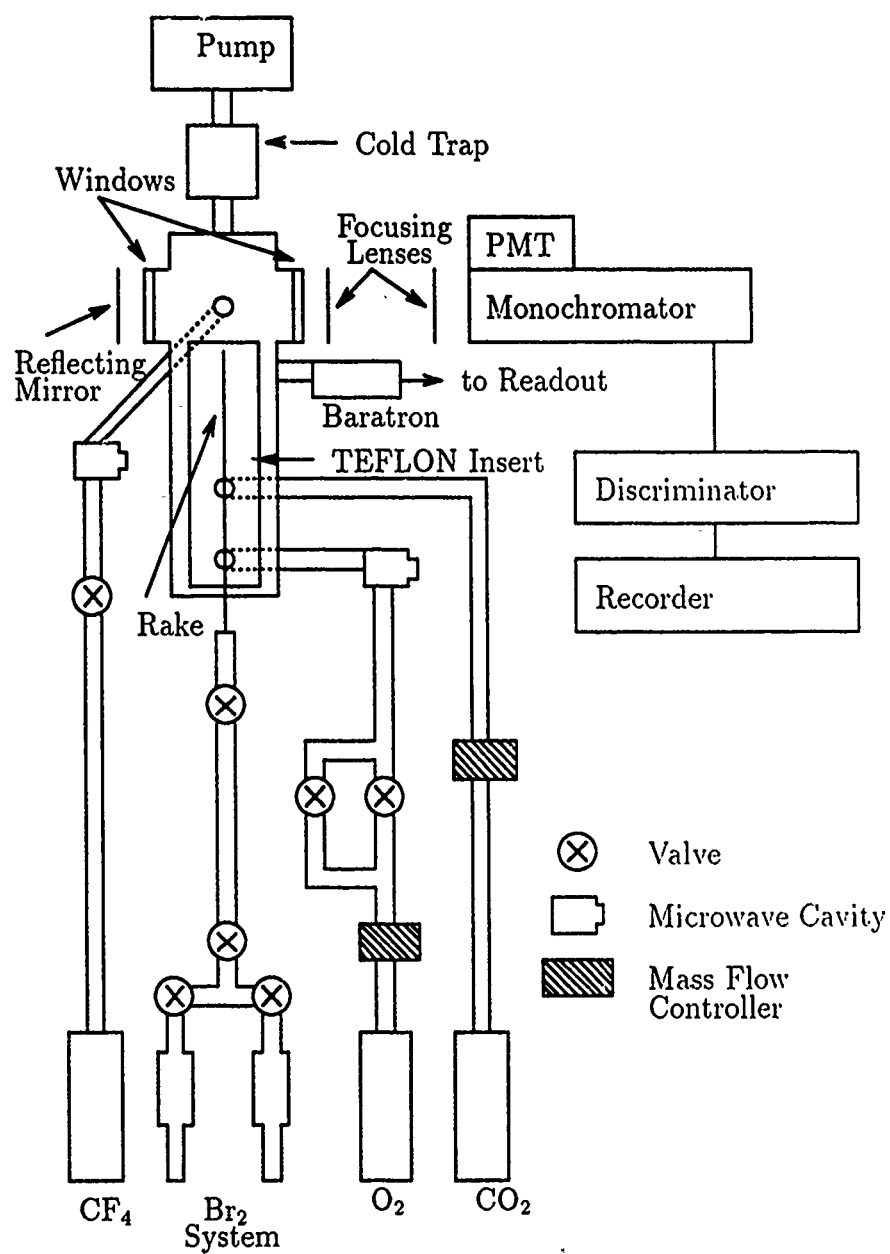
Gas flows (except Br_2) enter on the bottom of the tube.

Figure 5. Experimental Flow Tube Set Up

18

30 cm downstream from the microwave cavity. Their studies also indicate the atomic Fluorine concentration to be 3 to 10 times greater than the concentration of molecular Fluorine. The CF_4 concentration based on the valve calibration (Appendix C) is on the order of $2.0 \times 10^{16} \frac{molecules}{cm^3}$. Therefore, the F atom concentration in this set-up was then estimated to be on the order of $4.2 \times 10^{14} \frac{molecules}{cm^3}$.

A summary of these calculations leading to the calculated number densities of the reagents is listed in Table 7.

Table 7. Tabular Results of Reagent Number Densities

Reagent Species	$O_2(b)$	F	Br_2
Number Density (cm^{-3})	3-4x10^13	5-6x10^14	2x10^13

3.2 Chemiluminescence Spectra of BrF in the presence of Singlet Oxygen

Once production of BrF(B) was successfully maximized, experiments were conducted to examine the effect of varying the inputs on the BrF(B) emission, as well as the $O_2(b)$ emission. A continuous flow of reactants in the flow tube will be required to both generate the unstable species (the BrF(B) and singlet O_2) as well as produce the collisional excitation. The resulting emission will be spectrally resolved with a McPherson (0.3 m) grating monochromator and recorded with a RCA C31034A-02 photomultiplier tube and a Princeton Applied Research Model 1112 photon counting system(13). A lens focusing arrangement was placed between the output window of the flowtube to maximize the light being collected by the monochromator (see Figure 5). The first lens (f = 75mm) takes the diverging light rays coming out of the window and focuses them into parallel rays, while the second lens (f = 150mm) collects the parallel rays and focuses the rays to converge at the entrance slit of the monochromator. A small spherical mirror (diameter = 50mm) was placed next to the output window facing away from the monochromator to improve the recorded signal. A 30% increase in signal was recorded using this mirror, as opposed to not using the mirror. The first part of the experiment after successfully producing a

strong BrF(B) emission was to record the resulting emission spectrum in detail to ensure BrF(B) is the primary product in the flow producing an emission (other than the emission of $O_2(^1\Sigma)$), and to examine the spectrum to determine the relative vibrational populations of the B-state of BrF.

Six experiments were conducted to determine the dominant process in the excitation of BrF(B).

1. Observe the dependence of the BrF(B) emission on $O_2(^1\Sigma)$ using CO_2 as a selective quencher of $O_2(^1\Sigma)$.

2. Observe the emission of both BrF(B) and $O_2(^1\Sigma)$ as a function of changing Br_2 flow.

3. Observe the peak emission of BrF(B) as a function of changing CF_4 flow.

4. Observe the emission of $O_2(^1\Sigma)$ as a function of changing Br_2 flow (while not producing BrF). (Br_2 quenching of $O_2(^1\Sigma)$).

5. Observe the peak emission of both BrF(B) and $O_2(^1\Sigma)$ as a function of changing Br_2 flow with a reduction in the amount of O atoms in the system.

6. Observe the emission of $O_2(^1\Sigma)$ as a function of changing Br_2 flow with a reduction in the amount of O atoms in the system (while not producing BrF). (Br_2 quenching of $O_2(^1\Sigma)$).

Quenching experiments with CO_2 as a quenching species were used to determine the wall rate coefficients for experiments 2, 4, and 6.

First, the dependence of the BrF(B) emission was examined as a function of $O_2(b)$. CO_2 was used as a selective quencher of $O_2(b)$ since its quenching rate constant was known ($3.0 \times 10^{-13} cm^3/sec$ as shown from Section 2.3). The resulting plot of the $O_2(b)$ emission versus the BrF(B) emission as the amount of $O_2(b)$ in the system was reduced will show how the BrF(B) emission is dependent on $O_2(b)$.

Second, the production of BrF was conducted with a varying input flow of Br_2 molecules. This experiment was conducted starting with no Br_2 and gradually increasing the Br_2 flow, as well as with a high Br_2 flow gradually decreasing to no Br_2. The resulting plot of emission intensity versus Br_2 number density (and hence Br atom concentration) will show a relation between the BrF(B) emission and the O_2(b) emission as the excess Br_2 quenches the O_2(b).

Third, the production of BrF was repeated with a varying input flow of CF_4 (and therefore varying F atom concentration) to determine if the peak emission intensity changed with a different input of Br_2 flow. This procedure was used to determine the possibility of Br_2 number density (and hence Br atom concentration) changing as a result of changing F atom concentration. The resulting peak emission of BrF(B) as a function of changing CF_4 flow (and hence F atom concentration) compared to Br_2 number density will show a relation between Br and F atom concentration.

Fourth, the experiment was repeated simply by turning off the microwave discharge on the CF_4 inlet to remove production of F atoms and therefore determine the quenching of $O_2(^1\Sigma)$ by both Br atoms and Br_2 molecules. The resulting plot of emission intensity of $O_2(^1\Sigma)$ versus Br_2 number density will show the effect of the fast reactions of O atoms with Br_2 and BrO as outlined above.

Fifth, the experiment was conducted with the amount of O atoms in the system reduced and the resulting emission data plotted to determine the behavior of the emission as the population of O atoms is changed. The side branch of the O_2 inlet line had a quantity of Mercury (Hg) placed in a reservoir so that when the branch was opened, a coating of HgO will be applied downstream of the microwave cavity and hence reduce the amount of O atoms reaching the flow tube. Preliminary studies by Melton show that an HgO coating significantly reduces the amount of O atoms in the system (4). After this coating was applied for a set period of time, this branch was closed and the amount of O atoms then increased over time. (and as the HgO coating decays with time, the O atom population will increase). The emission of BrF(B) and

$O_2(b)$ was recorded both as the HgO coating was being applied as well as it decayed. The emission was recorded for sufficient time to show a significant change. The resulting behavior of the plot will show the relation between the recorded emission and the changing O atom population. (See Appendix A).

Sixth, the third experiment was repeated with the HgO coating applied to determine if a change in Br atom and Br_2 molecule quenching of $O_2(^1\Sigma)$ could be observed, and some insight into the amount of O atoms reduced by the HgO coating could be calculated.

Since the reaction mechanisms considered above include both singlet states of excited oxygen, quenching experiments were conducted to determine which of these two species (or both) is the primary contributor to pumping the BrF(B) by collisional energy transfer. Carbon dioxide (CO_2) will be used as a selective quencher of $O_2(^1\Sigma)$. Ranby and Rabek found that CO_2 has a significantly greater quenching rate constant for $O_2(^1\Sigma)$, $k_q = 3.3 \times 10^{-13}$ cm^3/molecule sec (16), versus Singh with that of $O_2(^1\Delta)$. $k_q = 0.5 \times 10^{-18}$ cm^3/molecule sec(18). Melton recorded comparable rate constants in his preliminary studies(26). During these experiments, the emission intensities of $O_2(^1\Sigma)$ and BrF were recorded as the CO_2 pressure is increased. The resulting plot of emission intensity versus CO_2 number density allows the background wall rates to be determined as well as the effect on BrF(B) emission as the amount of $O_2(^1\Sigma)$ is decreased.

3.3 Experimental·Calculations

Melton initially proposed determining the rate constant for the electronic quenching of singlet O_2 by BrF by examining the emission when the BrF is formed at the output of a variable position injector(4). From the flow tube set-up, the reaction time (t) can be calculated by dividing the distance from the injector to the observation port (D) by the bulk gas velocity ($\bar{v}$):

$$t = D/\bar{v} \tag{19}$$

Melton used Davis' study of the excitiation of IF(B) by singlet O_2 to calculate a similar quenching rate in the non-steady state (time dependent) regime[4, 24]. When the quenching species is in large excess relative to the other species, conditions approximating first order conditions are present and the resulting quenching rate is given by[4]:

$$k_q = \frac{(\Delta ln I(O_2^*))}{(\Delta[BrF])(t)} \tag{20}$$

where:

$I(O_2^*)$ represents the intensity of the excited oxygen emission.

$[BrF]$ represents the quenching species concentration.

t is the reaction time calculated above.

Characterization work carried out by Melton indicated that in this experimental arrangement, the time dependent regime cannot be accurately accessed due to the slow flow speeds (on the order of 1 to 2 m/sec) and the non-uniform spatial distribution caused by the shape of the rake[26]. Therefore, a steady state analysis (time independent) appeared to be the best way to resolve the quenching rate. Though this required taking the ratio of the quenching rate to the wall rate, Melton consistently recorded a wall rate (quenching) of singlet oxygen on the order of 50 sec^{-1}[26]. This results in a linear relation:

$$\frac{I_o}{I} = \frac{(k_q)([BrF])}{k_w} + 1 \tag{21}$$

23

or more explicitly,

$$k_q \;=\; \frac{(\{I_o/I\} - 1)(k_w)}{[BrF]} \tag{22}$$

where:

I_o represents the intensity of emission of excited oxygen with no quencher.

I represents the intensity of emission of excited oxygen in the presence of quencher.

$[BrF]$ represents the quenching species concentration.

k_q represents the quenching rate for BrF.

k_w represents the wall quenching rate during the production of BrF.

A similar analysis using CO_2 as the selective quencher of $O_2(^1\Sigma)$, because of its known quenching rate ($k_q = 3.0 \times 10^{-13}$ cm^3/molecule sec), will allow the wall rate, k_w, to be determined, and then used in the development above to calculate the k_q for the particular quenching species under investigation.

3.4 Excitation Analysis Procedure

Based on the data compiled during the experimental phase of this research, a detailed analysis of the excitation mechanism(s), reaction rate(s), and efficiency of this chemical process was possible. This analysis was accomplished in three steps.

1. The first step was to qualitatively determine which excitation path is responsible for the BrF emission based on a global view of the results.

2. The second step was to analytically determine the various pumping rates for the excitation and quenching rates for the involved gas species.

3. The third step was to analyze the efficiency of the system by looking at the ratios of the pumping rate to the quenching rate of the singlet oxygen.

IV. Results and Discussion

4.1 Vibrational Population Analysis

An examination of the relative vibrational level populations of the excited B-state of BrF was conducted by first taking a detailed spectrum of the BrF(B) emission in the flow tube. Figure 7 shows a typical spectrum from 5000 to 8000 Angstroms. The emission spectra showed good resolution for transitions in the range $5800 < \lambda < 7800$ Angstroms. Transitions at $\lambda < 5800$ Angstroms were not as clearly resolved due to overlap and the 0.7 nm resolution of the monochromator with $300\mu m$ slits (see Appendix C). The transitions observed matched those reported by Clyne. et al. (5) in their 1972 work. More detailed spectra are included in Appendix D. The relative vibrational populations were calculated from a comparison of the relative intensities for a particular transition (photons detected at each wavelength) which is proportional to the number density of the excited state (N_v). From an equation on relating the fluorescence intensity of a given rotational transition to the number density of the excited state (28):

$$I_{vw}^{emm} = (\frac{64\pi^4}{3})(c)(\nu_{vw})^4(q_{vw})|R_e|^2(\frac{S_J}{2J+1})(N_v) \tag{23}$$

where:

I_{vw}^{emm} = the emission intensity from state v to state w

ν_{vw} = transition frequency from state v to state w

q_{vw} = Franck-Condon Factor for transition from state v to state w

$|R_e|$ = rotational dipole moment

S_J = rotational linestrength factor

25

a conversion to examine the vibrational transitions using photon counting (the ν'^4 term becomes ν^3); as well as wavelength can be made (terms remaining relatively constant will be omitted):

$$I_{vw}^{emm} \propto (\nu_{vw})^3(q_{vw})(N_v) \qquad (24)$$

$$I_{vw}^{emm} \propto \frac{(q_{vw})(N_v)}{\lambda^3} \qquad (25)$$

The fraction of the photon intensity observed will depend on the spectral response of the PMT (See Appendix C.1). If the relative spectral response as a function of frequency $(D(\nu))$ is used, the actual observed emission intensity is then:

$$I_{vw}^{obs} = (I_{vw}^{emm})(D(\nu)) \qquad (26)$$

With the use of the analysis described in this section, the relative populations for each of the vibrational levels of BrF(B) can be calculated and then plotted. The resultant plot clearly shows that the population distribution is non-Maxwellian, see Figure 6. This directly leads to the conclusion that the production of BrF(B) in this system results in vibrationally hot BrF(B), with a considerable population not in the lowest vibrational energy level. A summary of these calculations are listed at Table 8.

Another way to examine the vibrational population distribution, this time obtaining an actual value for the population of each of the vibrational states of BrF(B) rather than the relative population distribution, was to take the ratios of the emission intensities for the clearly resolved transitions and compare them to the estimated population of $O_2(b)$; previously determined as $\approx 4 \times 10^{13}$ cm^{-3}.

Vibrational Level Population

NOTE: Plotted Points (diamonds) Reflect High, Average, And Low Values of the Relative Populations of v' Levels Based on Calculations

Maxwell-Boltzmann Distribution at 300 K
Potential Vibrational Distribution for BrF(B)
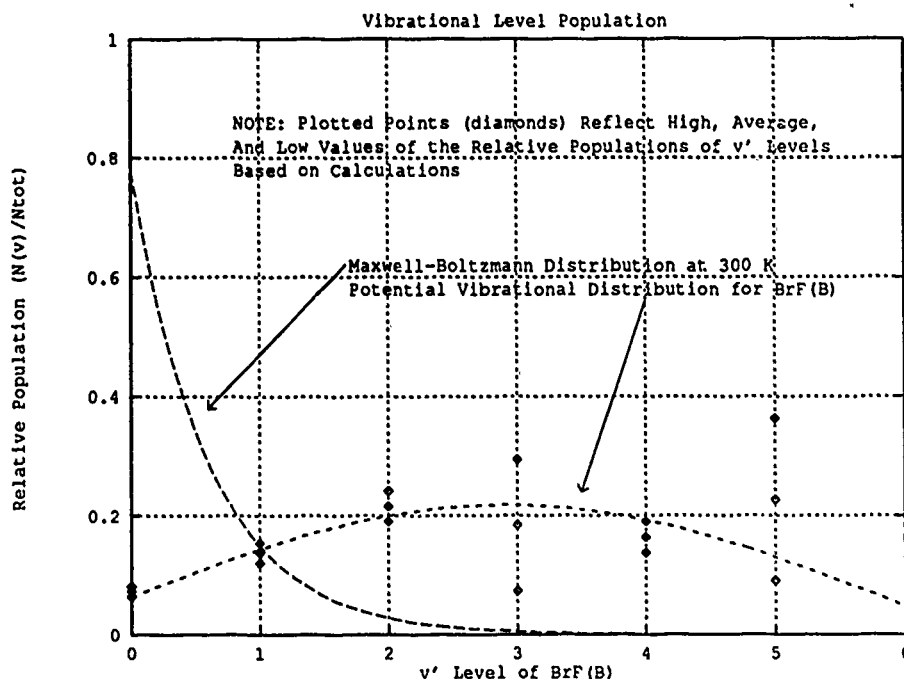
Figure 6. Relative Vibrational Population Distribution for BrF(B)

$$Pop(BrF(B)_v) = \Sigma_v \left(\frac{I^{emm}_{BrF(B)_v}(\tau_r)}{I^{emm}_{O_2(b)}(\tau_{rO_2(b)})}\right) Pop(O_2(b)) \tag{27}$$

where: $\tau_{rO_2(b)} = 12 secs$

τ_r is the radiative lifetime for a particular v-state of BrF(B)

$I^{emm} = I^{obs}/D$, where D is the spectral response

and the sum is over all clearly resolvable transitions at $\lambda > 5800\overset{\circ}{A}$

Then, taking the intensities observed on the recorded emission spectrum, the results obtained for the populations of the various v-levels of BrF(B) are shown in Table 9. The total calculated population for BrF(B) was determined to be 1.483×10^{10} cm^{-3}. The vibrational populations listed in Table 9 are determined by dividing the calculated population by the percent of the transitions whose Franck-

27

Table 8. Relative Vibrational Population Distribution for BrF(B)

v' Level	Maxwellian Relative N_v	Calculated Relative N_v	Error
0	0.8191	0.0726±0.0087	12%
1	0.1475	0.1372±0.0165	12%
2	0.0269	0.2158±0.0259	12%
3	0.0051	0.1836±0.1102	60%
4	0.0011	0.1636±0.0262	16%
5	0.0002	0.2271±0.1359	61%

Condon Factors are summed. (The values of all the Franck-Condon Factors for a transition originating at a particular v' sum to 1).

Table 9. Calculated Population of BrF(B)

BrF(B) v-state	# resolvable transitions	Calculated N_v (cm^{-3})	% FCF included	Vibrational N_v (cm^{-3})
v'= 0	5	4.83×10^8	.5141	9.395×10^8
v'= 1	6	8.62×10^8	.3829	22.512×10^8
v'= 2	5	12.32×10^8	.2767	44.525×10^8
v'= 3	6	11.28×10^8	.2905	38.830×10^8
v'= 4	5	6.57×10^8	.2080	31.587×10^8
v'= 5	1	3.43×10^7	.0222	15.450×10^8
Total				1.483×10^{10}

Then, the ratio of the total population of BrF(B) to $O_2(b)$ can be obtained from:

$$\frac{\Sigma_{all\ v} Pop(BrF(B))}{Pop(O_2(b))} = 3.71 \times 10^{-4} \tag{28}$$

This result is somewhat higher than would be predicted by Mechanism 1B (with the ratio of the estimated Br^* pumping rate over the Br^* quenching rate by $O_2(b)$):

$$[O_2(x)][F](k_{3-Body}) = (1.0 \times 10^{17})(6.0 \times 10^{14})(\sim 10^{-30}) = \sim 60 \qquad (29)$$

$$[O_2(x)](k_q) = (1.0 \times 10^{17})(2.8 \times 10^{-11}) = \sim 2.8 \times 10^6 \qquad (30)$$

$$then \ 60/2.8x10^6 \approx 2.1 \times 10^{-5} \qquad (31)$$

$$(32)$$

where k_q is the Br atom quenching rate constant on $O_2(b)$

This quenching rate constant is determined in Section 4.2. No predictions about the behavior of Mechanism 1A or 2 were possible since the pumping rate to the intermediate state (BrF*) was not determined.

4.2 Analysis of Chemiluminescence Experiments

The first experiment examined the BrF(B) emission dependence on $O_2(b)$. Numerous repetitions showed that the BrF(B) emission signal varied almost linearly with the amount of $O_2(b)$; as determined by comparing Io/I for both the BrF(B) and $O_2(b)$ emission signals. The conclusion drawn from this data is that the BrF(B) pumping mechanism requires a single interaction with $O_2(b)$. This behavior is shown in Figure 8. The slight curvature observed in this plot might be due to some quenching of the excited intermediate state of BrF.

The second experiment recorded the emission of both BrF(B) and $O_2(b)$ as a function of changing Br_2 flow. The peak BrF(B) signal was observed at a Br_2 number density of $2.00 \pm 0.05 \times 10^{13}$ cm^{-3}. This behavior is shown in Figure 9. The implications of this observation with respect to the 3-Body Mechanism are as follows:

- The peak BrF(B) signal would occur at the point where the Br_2 number density equaled two times the O atom number density.
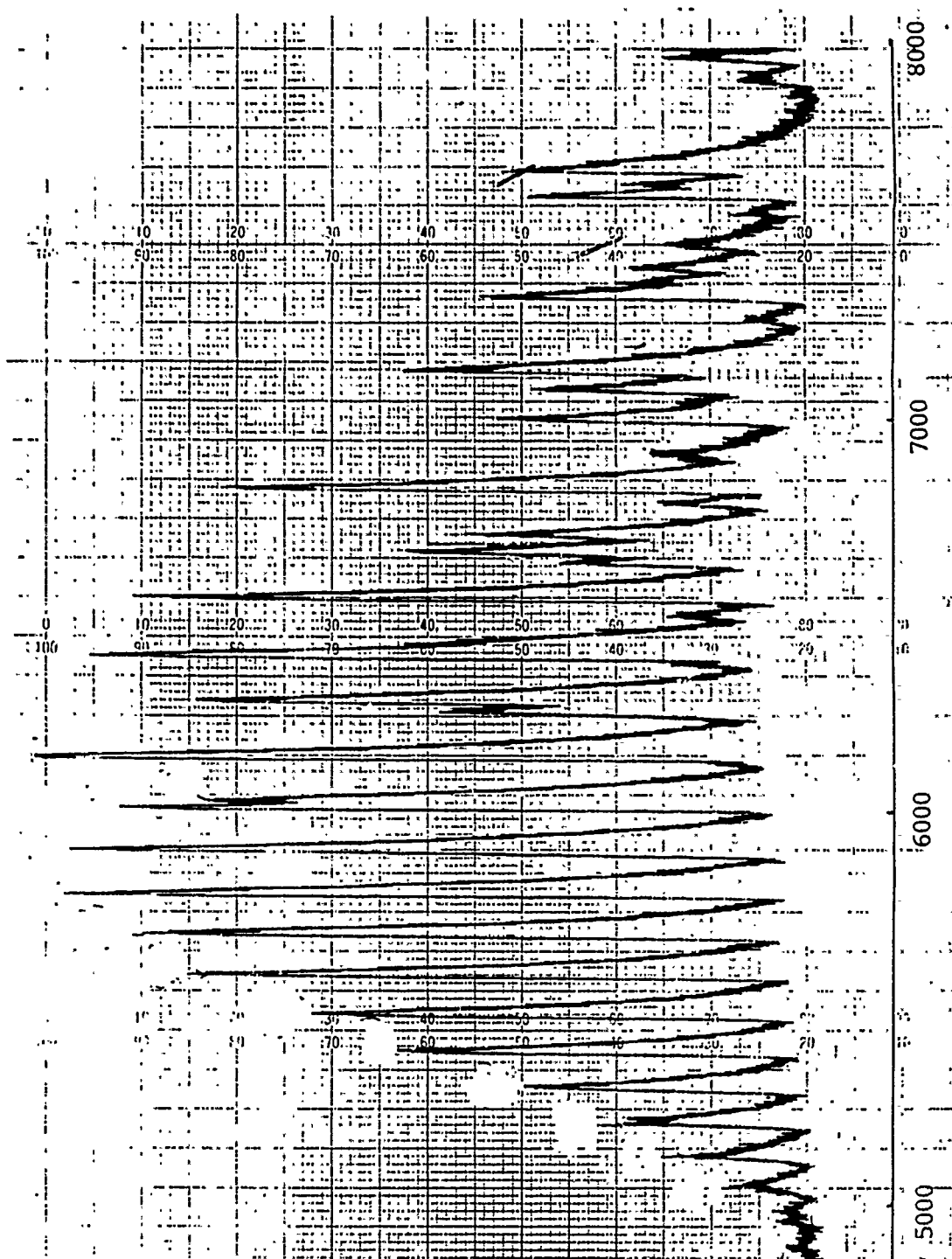
29

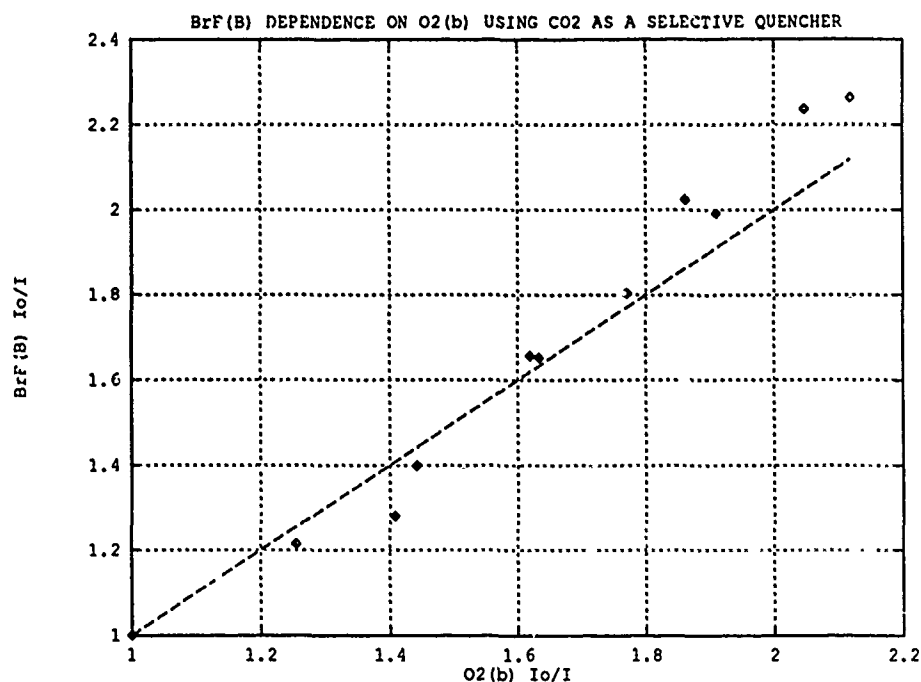Figure 7. Emission Spectrum of BrF(B) Excited By $O_2(b)$

Figure 8. BrF(B) Dependence on O_2(b)

- Additional Br_2 added to the system beyond the peak would remove F atoms thus decreasing the BrF(B) signal.

- The increased Br atoms produced as a result of the F + Br_2 reaction would quench the O_2(b) signal, also contributing to the decrease in BrF(B) signal.

The implications of this observation with respect to the 2-Step Mechanism are as follows:

- The peak of the BrF(B) signal would occur at the point where the Br_2 number density equaled the F atom number density.

- Additional Br_2 added to the system beyond the peak would quench the O_2(b) thus reducing both the BrF(B) and O_2(b) signals.

Since in the earlier discussion on BrF production it was determined that the number density of F atoms was an order of magnitude larger than the number density of Br_2 at the point of producing an optimum signal, these results would seem to

31

indicate that the 2-Step Mechanism is incorrect. A second part to this experiment was to examine the behavior of the decay of the BrF(B) and O_2(b) signal beyond the peak emission point. It was observed that the BrF(B) signal drops at a significantly greater rate than the O_2(b) signal. This behavior is illustrated in Figure 10. An O_2(b) decay constant of $k_1 = 3.2 \times 10^{-11}$ cm^3/sec was calculated from the slope of the line fit to the decay curve for O_2(b). If the 2-Step Mechanism were correct, the expected behavior would be for the BrF(B) and O_2(b) signals to drop off together. The 3-Body Mechanism would cause the BrF(B) signal to totally disappear when the Br_2 number density equaled the F atom number density because no F atoms would be left to contribute to the 3-body collisional process. At the right side of the plot, the Br_2 number density of $\sim 2.0 \times 10^{14}$ cm^{-3} is approaching the F atom number density of $\sim 4.0 - 6.0 \times 10^{14}$ cm^{-3}. Since the 3-Body Mechanism explains this divergence of the BrF(B) signal with respect to the O_2(b) signal, this observation would tend to support that mechanism.
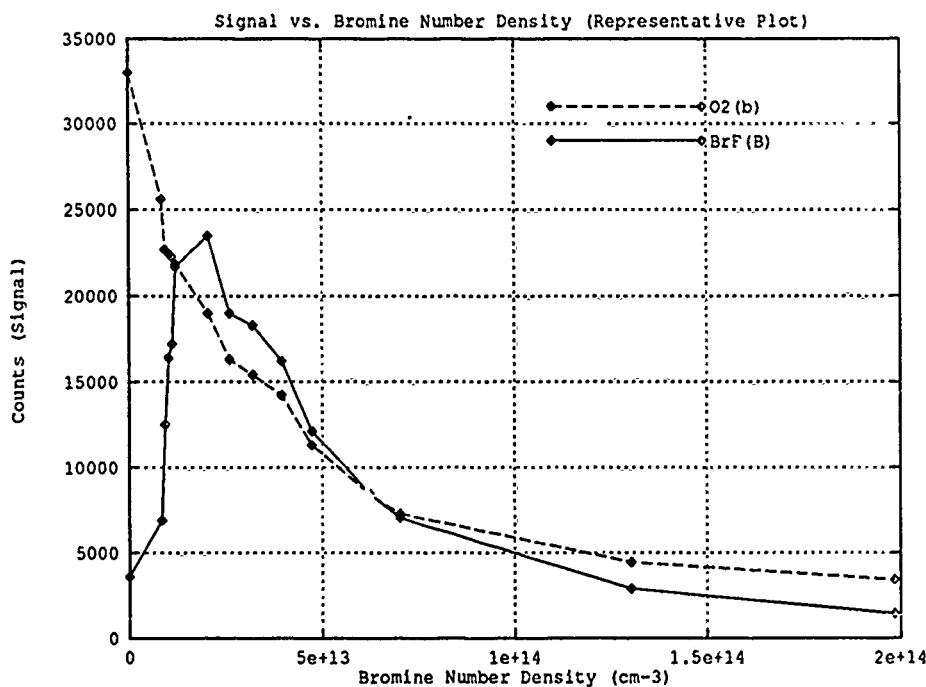

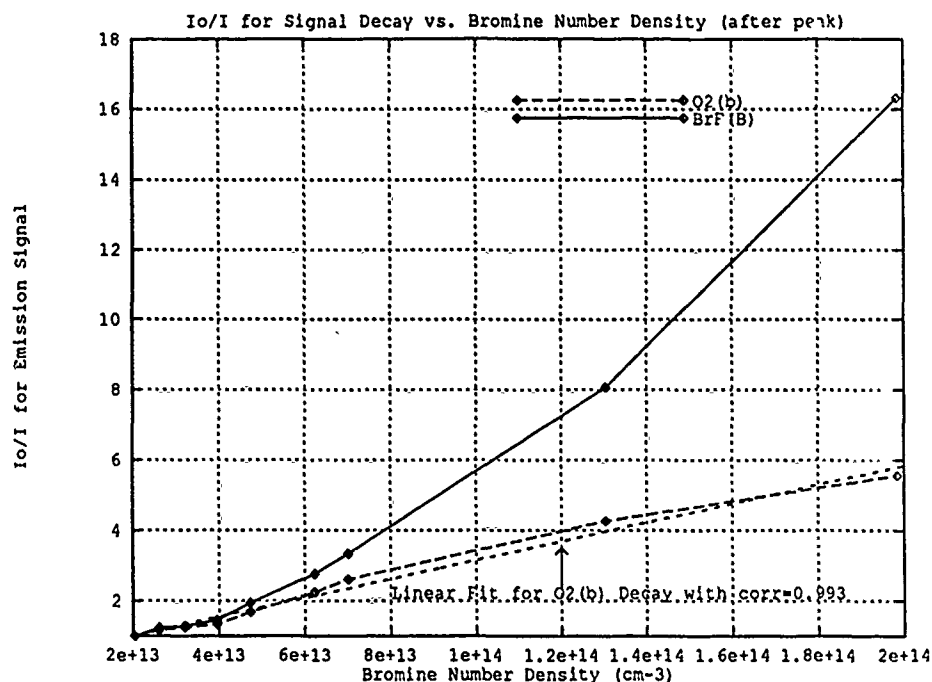Figure 9. Signal vs. Br_2 Number Density

Figure 10. Io/I Plot: Signal Decay (after peak) vs. Br₂ Number Density

The third experiment observed the peak emission of BrF(B) as a function of changing the CF$_4$ flow. While the actual strength of the BrF(B) signal changed when the flow rate of CF$_4$ was altered, the input number density of Br$_2$ remained unchanged. The CF$_4$ flow rates in this experiment were varied from 100 to 300 sccm, with the maximum BrF(B) signal being obtained at 190 sccm, just as in the prvious experiments. Since the Br$_2$ number density remained stable throughout these experiments, the 3-Body Mechanism would indicate that the Br$_2$ number density is then dependent on the number of O atoms present in the flow tube system. In the 2-Step Mechanism, changing the number of F atoms in the system should show a definite change in the amount of Br$_2$ needed to produce a maximum signal of BrF(B). Although the exact efficiency of the microwave cavity as a function of changing CF$_4$ flow was not calculated, it is clear that changing the CF$_4$ flow rate will change the F atom concentration. The results of this experiment are consistent with the 3-Body Mechanism, but really cannot support any conclusion about the 2-Step Mechanism.

The fourth experiment was to observe the emission of $O_2(b)$ as a function of changing Br_2 flow. In this case, all conditions remained the same except the CF_4 microwave discharge was turned off. Therefore, there was no F atom production. Also, since the CF_4 flow was not changed, the CF_4 quenching rate constant of $k_{CF_4} = 2.68 \times 10^{-15}$ cm^3/sec (as experimentally verified by Melton (4)) was included as part of the background wall rate when the Br and Br_2 quenching rate constants were calculated. The behavior of the $O_2(b)$ signal as the Br_2 number density was changed is illustrated in Figure 11. Two critical observations from this experiment were the quenching rate changed abruptly at a Br_2 number density of 2.0×10^{13} cm^{-3} and this was the same number density where the peak emission signal for $BrF(B)$ in the first experiment. An importance inference drawn from this behavior was that since no F atoms were present in the system, this behavior must be attributed to O atoms. Only the 3-Body Mechanism can support these observations.
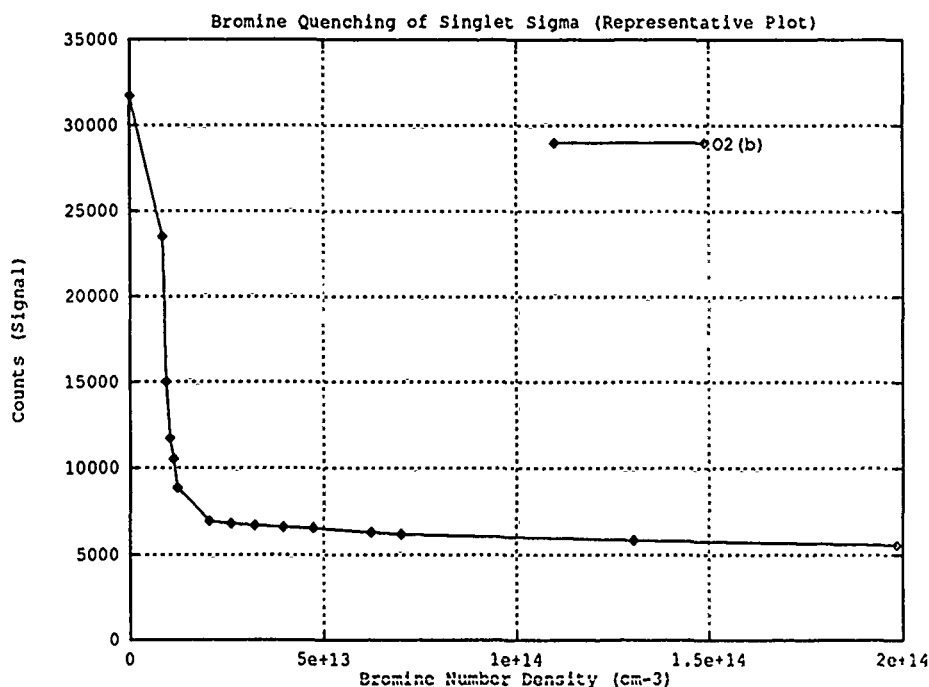

Figure 11. Br_2 Quenching of $O_2(^1\Sigma)$

Two questions can be answered regarding the decay of the $O_2(b)$ signal by an examination of the behavior of the plot. The results from the previous plot were

34

changed to I_o/I for the $O_2(b)$ signal vs. Br_2 number density so the quenching rate constants could be calculated. This is illustrated in Figure 12.

Bromine Quenching of Singlet Sigma (Representative Plot)

Fit Denoting Br2 Quenching, k(Br2)=9.7x10E-13 cm3/sec
Fit Denoting Br Quenching, k(Br)=2.8x10E-11 cm3/sec
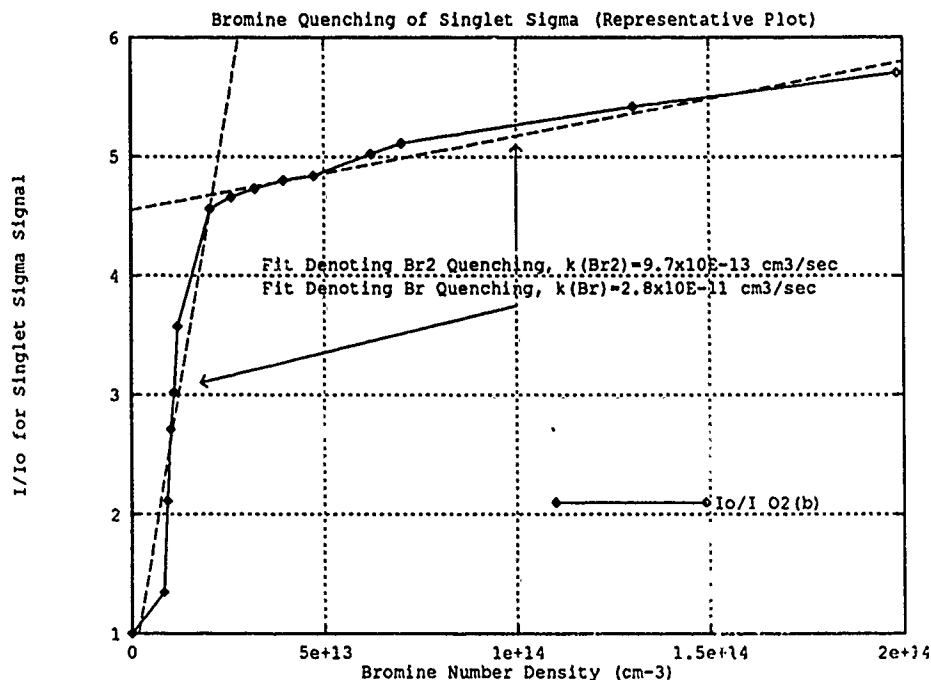
Io/I O2(b)

Bromine Number Density (cm-3)

Figure 12. I_o/I Plot: Br_2 Quenching of $O_2(^1\Sigma)$

First, what caused the behavior in the second decay region? The second decay region must have been caused due to Br_2 quenching of $O_2(b)$. Since the O_2 flow mixed upstream with the Br_2 flow before it reached the output window, the Br_2 reacted at a gas kinetic rate with the O atoms present in the O_2 flow to produce one Br atom for every O atom (as previously developed in the rate equations). Therefore, the dramatic change in slope was caused when the number of Br_2 molecules equaled twice the number of O atoms. Until this point was reached, there were no surviving Br_2 molecules in the flow. A Br_2 quenching rate constant of $k_{Br_2} = 9.7 \pm 0.5 \times 10^{-13}\ cm^3/sec$ was calculated, which is $\sim 1/30$ of the rate, k_1, derived in the first experiment. If the 2-Step Mechanism were correct, no BrF(B) signal would be seen until there were Br_2 molecules in the flow at the previously recorded number density of $2.0 \times 10^{13}\ cm^{-3}$. Only the 3-Body Mechanism is consistent with the observed BrF(B) emission increasing with increasing Br_2 up to $2.0 \times 10^{13}\ cm^{-3}$.

Second, what caused the behavior in the first decay region? The first decay region must have been caused by Br atom quenching of $O_2(b)$. In this region, where the amount of Br_2 is less than two times the amount of O atoms, the increasing species must be Br atoms. The gas kinetic reactions of Br_2 with O atoms resulting in two Br atoms and an O_2 molecule again dominated, allowing no free Br_2 molecules until $Br_2 > 2(O)$. A Br atom quenching rate constant of $k_{Br} = 2.8\pm0.3\times10^{-11}$ cm^3/sec was calculated. Since the Br atoms quench $O_2(b)$ (perhaps deexciting down to $O_2(a)$), a possibility exists for energy transfer to take place. The energy gap between $Br(^2P_{1/2})$ and $Br(^2P_{3/2})$ differs from that of $O_2(b)(v'=0)$ and $O_2(a)(v'=1)$ by 69 cm^{-1}, a very small difference. This observation may indicate that some electronically excited Br atoms are produced, suggesting the possibility of the variant to the 3-Body Mechanism. (The same behavior as discussed above was observed in the sixth experiment, where the amount of O atoms were reduced in the system, and comparable Br and Br_2 quenching rate constants were determined).

The fifth experiment recorded the peak emission of both BrF(B) and $O_2(b)$ while the O atom population in the system was changed. The O atom population was reduced while the HgO coating was applied, and then increased as the HgO coating decayed away. The $O_2(b)$ signal changed significantly more than the BrF(B) signal. On average, with a 30 minute application of HgO coating, the $O_2(b)$ signal would increase by a factor of 4, while the BrF(B) signal increased by about 50 percent. The behavior observed was that the BrF(B) signal tended to increase linearly with the $O_2(b)$ signal as O atoms were reduced, and likewise decrease as the O atoms increased.

The rate equation development in Appendix A was used to analyze these results. The slopes recorded were on average slightly greater than zero. This behavior is illustrated in Figure 13.
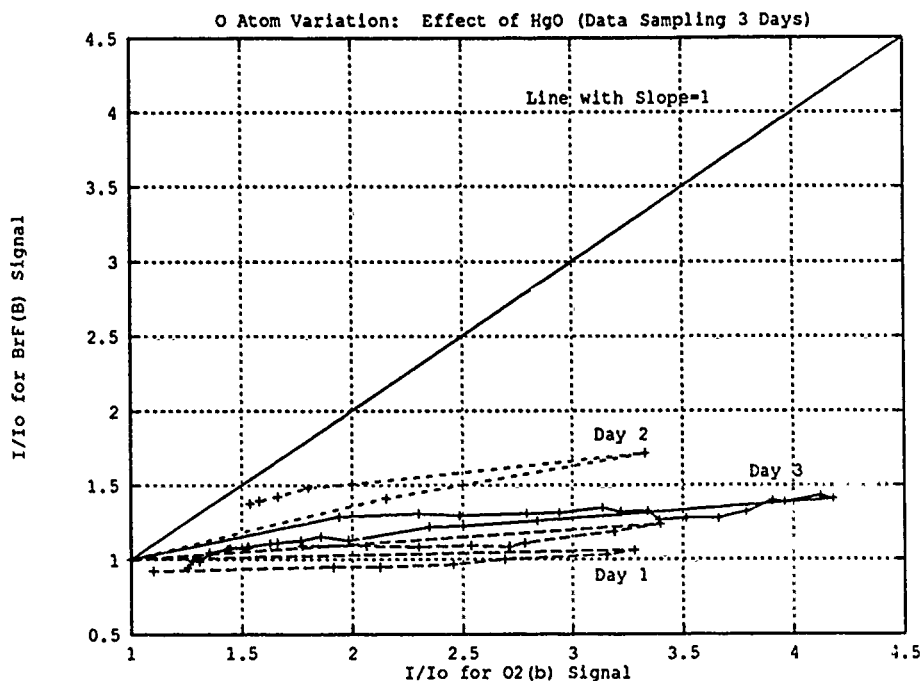
Figure 13. I/Io Plot: O Atom Effect on Emission

The final forms of the rate equations for the 3-Body and 2-Step Mechanisms will be repeated here for ease of understanding.

$$\frac{1}{y} = \frac{1}{x}(1 - \frac{\beta}{Br_{max}}) + \frac{\beta}{Br_{max}} \tag{33}$$

$$\frac{1}{y} = \frac{1}{x}(1 + \frac{2\beta}{BrF(X)_{min}}) - \frac{2\beta}{BrF(X)_{min}} \tag{34}$$

For the 3-Body Mechanism with the excited intermediate state of BrF, it is assumed the production of BrF(B) and BrF* are in steady-state, $O_2(x)$ is quenching BrF*, and whatever Br atoms in the system are quenching $O_2(b)$. For the 3-Body Mechanism with the electronically excited Br atoms, the same assumptions hold except it is assumed that $O_2(x)$ is quenching Br*. The first rate equation listed above would predict that a slope of less than 1 would be observed, and that is in fact the observed behavior in this experiment. This information supports the 3-Body Mechanism, but cannot differentiate between either of the variants suggested. For

37

the 2-Step Mechanism, the same assumptions hold as in the first example above. The second rate equation listed above would predict that a slope greater than 1 would be observed. Since this was not the observed behavior, this information would tend to discount the 2-Step Mechanism.
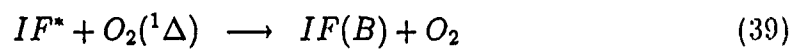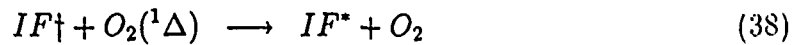
4.3 Comparison to Iodine Monofluoride

This section will highlight some of the previously conducted work on IF by S. Davis, et al. Davis and his colleagues conclusively achieved excitation of IF(B) by $O_2(^1\Sigma, ^1\Delta)$ in a fast flow reactor (24). Their initial work with vibrationally cold IF(X) showed that the IF(B) produced had a linear relationship to the amount of $O_2(^1\Sigma)$. If they had vibrationally excited IF(X)(v>> 0), the IF(B) emission was enhanced by two orders of magnitude and changes in the amount of $O_2(^1\Sigma)$ had little, if any, effect on this emission (24). This led them to believe that a 2-Step Mechanism to an intermediate excited state of IF, here called IF*, with sequential collisions of $O_2(^1\Sigma)$ and $O_2(^1\Delta)$ was the primary pumping channel, even if inefficient. This is illustrated below:

$$IF(X) + O_2(^1\Sigma) \longrightarrow IF^* + O_2 \tag{35}$$

$$IF^* + O_2(^1\Delta) \longrightarrow IF(B) + O_2 \tag{36}$$
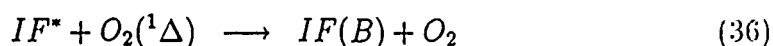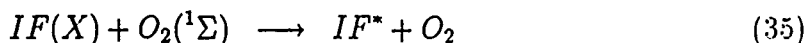
Their continued work looking at multiple collisions with $O_2(^1\Delta)$ showed that this 2-Step Mechanism dominates any 3-Body Mechanism, but that vibrationally excited IF(X)(v>> 0) was required (25). They used a number of techniques to produce vibrationally excited IF, here called IF†. Then, sequential collisions with $O_2(^1\Delta)$ gave a very strong IF(B) emission. Their evidence reveals some intermediate excited state of IF, called IF* is needed as a reservoir state. This is illustrated as:

$$IX + F \longrightarrow IF\dagger + F \tag{37}$$

$$IF\dagger + O_2(^1\Delta) \longrightarrow IF^* + O_2 \qquad (38)$$

$$IF^* + O_2(^1\Delta) \longrightarrow IF(B) + O_2 \qquad (39)$$

While Davis and his colleagues have not reported any rate constants as yet, their work continues in this aspect. They did conclude that IF(X,v$\geq$ 9) is an important factor in the excitation of IF(B) by $O_2(^1\Delta)$ (25).

V. Conclusions and Recommendations

5.1 Conclusions

The chemiluminescence spectra obtained in this research proved conclusively that BrF(B) can be produced by $O_2(^1\Sigma)$ pumping. The resulting vibrational distribution for BrF(B) was shown to be non-Maxwellian (non-thermal). The BrF(B) chemiluminescence spectral analysis clearly identified transitions from BrF(B)(v'= 0,1,2,3,4,5) with some possible transitions from BrF(B)(v'= 6) although these could not be clearly resolved. The transitions from v'= 6 are less likely due to predissociation at the higher rotational levels.

The analyzed data suggests strongly that some type of 3-Body Mechanism produces BrF(B), although the exact pumping process could not be distinguished. Although Davis postulates a 2-Step Mechanism for IF (another interhalogen) pumping by $O_2(^1\Sigma)$ (2, 24), this process was not observed with BrF. The determined pumping efficiency of 3.7×10^{-4} leads to the conclusion that $O_2(^1\Sigma)$ pumping is relatively inefficient and therefore perhaps a poor choice of excitation energy for a BrF laser. However, since the 3-Body recombination rate was not determined in this research, a conclusive statement cannot be made regarding the potential of $O_2(b)$ pumping for a BrF laser.

The quenching rates for $O_2(^1\Sigma)$ by CO_2, CF_4, Br, and Br_2 were also determined. The CO_2 and CF_4 quenching rates were comparable to previously recorded work. The Br and Br_2 quenching rates have not been previously recorded.

5.2 Recommendations

The work started with this research to determine the rate constants for BrF should be continued. Some recommendations are made for further work in this area.

Readjusting the flow tube set-up for a linear geometry would allow the 3-Body reaction rate to be more accurately determined. This would entail injecting the F atoms down the center of the flow tube (through the rake) after the O_2 and Br_2 flows had been mixed upstream. A better value for the 3-Body recombination rate constant (other than the estimate used in the analysis of this research) would allow an improved determination of the efficiency of the system. Once this constant were known, then a look at the ratio of the pumping rate from the intermediate state vs. the quenching rate of the intermediate state would better indicate the efficiency of the system.

More accurate flow meters are required for precise control of the reagent gases used in the rate determination experiments. The Sierra Instruments Mass Flow Controllers are not sensitive enough for the low number density of the Br_2 flow.
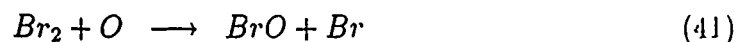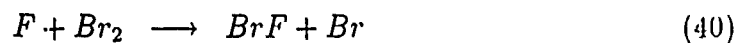
Using F_2 in a bath gas of He could be used to increase the number of F atoms available for reaction as well as to determine a more accurate number density of F mixing in the system. This gas was not available during the course of this research, which necessitated the use of dissociated CF_4 as the source of F atoms.

Incorporating more TEFLON tubing in the system after the microwave cavities would decrease the wall quenching effects. Although a TEFLON insert was used in the flow tube itself to reduce wall quenching effects, a greater use of TEFLON tubing could reduce this effect more.

If further studies show $O_2(b)$ to be unsuitable as an energy source for production of $BrF(B)$, then an examination of another metastable molecule as an energy carrier may prove profitable.
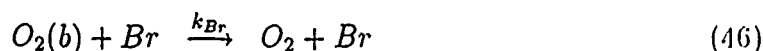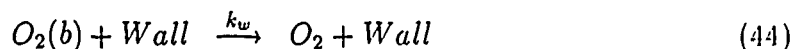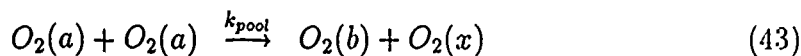
Appendix A. Rate Equations in the Presence of Atomic Oxygen

The basic reaction in producing BrF as well as the reaction of Br_2 with O atoms are the fast reactions:

$$F + Br_2 \longrightarrow BrF + Br \qquad (40)$$

$$Br_2 + O \longrightarrow BrO + Br \qquad (41)$$

$$BrO + O \longrightarrow Br + O_2 \qquad (42)$$

These reactions occur at a gas kinetic rate. In the flow tube apparatus of this experiment, these reactions essentially take place instantaneously. The combined effect of the O atom reactions show that for every two O atoms, two Br atoms are produced.

The production of singlet oxygen is determined by the following rate equations. which include the pooling reaction of $O_2(a)$, the quenching of $O_2(b)$ due to the walls (and other reagents), and the quenching of $O_2(b)$ due to O atoms and Br atoms:

$$O_2(a) + O_2(a) \xrightarrow{k_{pool}} O_2(b) + O_2(x) \qquad (43)$$

$$O_2(b) + Wall \xrightarrow{k_w} O_2 + Wall \qquad (44)$$

$$O_2(b) + O \xrightarrow{k_o} O_2 + O \qquad (45)$$

$$O_2(b) + Br \xrightarrow{k_{Br}} O_2 + Br \qquad (46)$$

Where:

$$\frac{dO_2(b)}{dt} = k_{pool}(O_2(a))^2 - k_w O_2(b) - k_o O_2(b)(O) - k_{Br} O_2(b)(Br) \qquad (47)$$

And since experimental results indicate that $k_o \ll k_{Br}$, the O atom quenching of $O_2(b)$ will be considered small with respect to the Br atom quenching, and neglected in the following development. Then, in steady state analysis where $dO_2(b)_o/dt = 0$ is the case for initial conditions prior to removing O atoms (where the number of Br atoms is a maximum: Br_{max}), and in the case after some O atom removal where $dO_2(b)/dt = 0$ (where the number of Br atoms is a minimum: $Br_{max} - \Delta Br$):

$$O_2(b)_o = \frac{k_{pool}(O_2(a))^2}{k_w + k_{Br}(Br_{max})} \qquad (48)$$

$$O_2(b) = \frac{k_{pool}(O_2(a))^2}{k_w + k_{Br}(Br_{max} - \Delta Br)} \qquad (49)$$

$$\frac{O_2(b)_o}{O_2(b)} = \frac{k_w + k_{Br}(Br_{max} - \Delta Br)}{k_w + k_{Br}Br_{max}} \qquad (50)$$

$$\frac{O_2(b)_o}{O_2(b)} = 1 - \frac{k_{Br}(\Delta Br)}{k_{w'}} \qquad (51)$$

$$(\Delta Br) = (1 - \frac{O_2(b)_o}{O_2(b)})(\frac{k_{w'}}{k_{Br}}) \qquad (52)$$

Where $k_{w'}$ has been used as the combined effect of the walls and baseline Br concentration. These results will be used later. NOTE: The explicit forms for concentrations of species have been omitted for clarity in this and the following developments. For example: the concentrations of [O] and [O_2], will simply be written as O and O_2.

More explicitly, the following table will illustrate the effect on the differing reagents as the O atom population is changed due to the HgO coating (the HgO coating removes some amount of O atoms):

43

Case with No HgO Coating Applied	Case with HgO Coating Applied
Greatest # of O atoms	Least # of O atoms
Therefore greatest # of Br atoms	Therefore least # of Br atoms
Therefore least # of Br_2	Therefore greatest # of Br_2
Results in least BrF(X)	Results in most BrF(X)
In terms of Δ's	In terms of Δ's
O_{max}	$O_{max} - \Delta O$
Br_{max}	$Br_{max} - \Delta Br$
Br_{2min}	$Br_{2min} + \Delta Br_2$
$BrF(X)_{min}$	$BrF(X)_{min} + \Delta BrF(X)$

Then, in terms of the relationship between all of the changes in species, the following equality holds: $|\Delta BrF| = |\Delta Br_2| = |\Delta 2O| = |\Delta 2Br|$.

A 3-body mechanism (two variants) and a 2-step mechanism are considered to be potentially responsible for the excitation of BrF(B). These two mechanisms will be explicitly developed in this section. The first mechanism is the 3-body mechanism:

$$Br + F + O_2(x) \xrightarrow{k_1} BrF^* + O_2(x) \tag{53}$$

$$BrF^* + O_2(b) \xrightarrow{k_2} BrF(B) + O_2(x) \tag{54}$$

$$BrF^* + O_2(x) \xrightarrow{k_q} BrF(X) + O_2 \tag{55}$$

$$BrF(B) + O_2(x) \xrightarrow{k_3} BrF(X) + O_2 \tag{56}$$

$$BrF(B) \xrightarrow{1/\tau_r} BrF(X) + h\nu \tag{57}$$
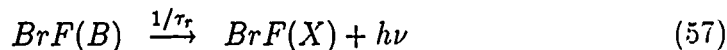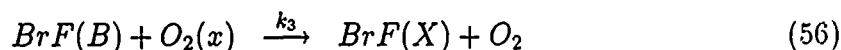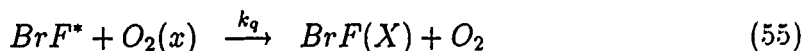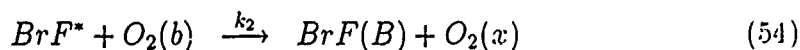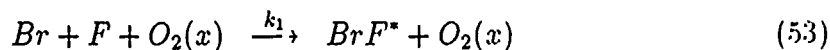
(where $O_2(x)$ is a third body and BrF^* is an excited intermediate state)

Then,

$$\frac{dBrF^*}{dt} = FBrO_2(x)k_1 - BrF^*(k_2O_2(b) + k_qO_2(x)) \qquad (58)$$

$$\frac{dBrF(B)}{dt} = k_2BrF^*O_2(b) - BrF(B)(k_3O_2(x) + (1/\tau_r)) \qquad (59)$$

And in steady state, where $dBrF^*/dt = 0$ and $dBrF(B)/dt = 0$:

$$BrF^* = \frac{FBrO_2(x)k_1}{k_2O_2(b) + k_qO_2(x)} \qquad (60)$$

$$BrF(B) = \frac{k_2BrF^*O_2(b)}{k_3O_2(x) + (1/\tau_r)} \qquad (61)$$

Resulting in a combined form, for both a greater amount of O atoms ($BrF(B)_o$) and a lesser amount of O atoms ($BrF(B)$), of:

$$BrF(B) = \frac{F(Br_{max} - \Delta Br)O_2(x)O_2(b)k_1k_2}{(k_2O_2(b) + k_qO_2(x))(k_3O_2(x) + (1/\tau_r))} \qquad (62)$$

$$BrF(B)_o = \frac{FBr_{max}O_2(x)O_2(b)_ok_1k_2}{(k_2O_2(b)_o + k_qO_2(x))(k_3O_2(x) + (1/\tau_r))} \qquad (63)$$

$$\frac{BrF(B)_o}{BrF(B)} = \left(\frac{O_2(b)_o}{O_2(b)}\right)\left(\frac{Br_{max}}{Br_{max} - \Delta Br}\right)\left(\frac{k_2O_2(b) + k_qO_2(x)}{k_2O_2(b)_o + k_qO_2(x)}\right) \qquad (64)$$

$$\frac{BrF(B)_o}{BrF(B)} = \frac{O_2(b)_o}{O_2(b)}\left(\frac{Br_{max}}{Br_{max} - \Delta Br}\right)\left(\frac{k_2O_2(b) + k_qO_2(x)}{k_2O_2(b)_o + k_qO_2(x)}\right) \qquad (65)$$

Simplifying this expression by using $y = BrF(B)_o/BrF(B)$, $x = O_2(b)_o/O_2(b)$, and using a substitution for $(\Delta Br) = (1 - x)(k_{w'}/k_{Br})$ from above, gives:

$$y = x\left(\frac{Br_{max}}{Br_{max} - (1 - x)(k_{w'}/k_{Br})}\right)\left(\frac{(1/x)\left(\frac{O_2(b)_ok_2}{O_2(x)k_q}\right) + 1}{\left(\frac{O_2(b)_ok_2}{O_2(x)k_q}\right) + 1}\right) \qquad (66)$$

45

This expression can be simplified further by setting:

$$\alpha = \frac{O_2(b)_o k_2}{O_2(x) k_q} \tag{67}$$

$$\beta = \frac{k_{w'}}{k_{Br}} \tag{68}$$

$$y = x\left(\frac{Br_{max}}{Br_{max} - \beta(1-x)}\right)\left(\frac{(1/x)\alpha + 1}{\alpha + 1}\right) \tag{69}$$

$$y = x\left(\frac{1}{1 + \beta(1/Br_{max})(x-1)}\right)\left(\frac{(1/x)\alpha + 1}{\alpha + 1}\right) \tag{70}$$

Now, assuming that α is small (on the order of 10^{-3}) because the concentration of $O_2(b)_o$ is much less than the concentration of $O_2(x)$, as well as $k_2 < k_q$; and then inverting the equation:
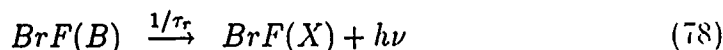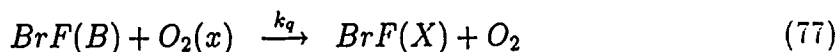
$$y = x\left(\frac{1}{1 + (x-1)\frac{\beta}{Br_{max}}}\right) \tag{71}$$

$$\frac{1}{y} = \frac{1}{x}\left(1 + (x-1)\frac{\beta}{Br_{max}}\right) \tag{72}$$

$$\frac{1}{y} = \frac{1}{x}\left(1 - \frac{\beta}{Br_{max}}\right) + \frac{\beta}{Br_{max}} \tag{73}$$

The last equation showing clearly that the slope of the line of the ratios of $1/y$ to $1/x$ will be less than or equal to 1, with an intercept greater than or equal to 0.

A variant of the 3-Body Mechanism illustrated above postulates the formation of excited Br atoms by resonant collisional energy transfer with $O_2(b)$, and then formation of BrF(B) through third body collision. An abbreviated development of the rate equations in the same form follows:

46

$$Br + O_2(b) \xrightarrow{k_{Br}} Br^* + O_2(a) \tag{74}$$

$$Br^* + F + O_2(x) \xrightarrow{k_1} BrF(B) + O_2(x) \tag{75}$$

$$Br^* + O_2(x) \xrightarrow{k_2} Br + O_2 \tag{76}$$

$$BrF(B) + O_2(x) \xrightarrow{k_q} BrF(X) + O_2 \tag{77}$$

$$BrF(B) \xrightarrow{1/\tau_r} BrF(X) + h\nu \tag{78}$$

Then, repeating the steady-analysis for dBrF(B)/dt = 0 and dBr*/dt = 0:

$$BrF(B) = \frac{FBR^*O_2(x)k_1}{k_q O_2(x) + 1/\tau_r} \tag{79}$$

$$Br* = \frac{BrO_2(b)k_{Br}}{k_2 O_2(x) + FO_2(x)k_1} \tag{80}$$

Giving in combined form, for both cases of greater or lesser amounts of O atoms:

$$BrF(B) = \frac{FBr_{min}O_2(x)O_2(b)k_1 k_{Br}}{(k_q O_2(x) + 1/\tau_r)(k_2 O_2(x) + FO_2(x)k_1)} \tag{81}$$

$$BrF(B)_o = \frac{FBr_{max}O_2(x)O_2(b)_o k_1 k_{Br}}{(k_q O_2(x) + 1/\tau_r)(k_2 O_2(x) + FO_2(x)k_1)} \tag{82}$$

$$\frac{BrF(B)_o}{BrF(B)} = \frac{O_2(b)_o}{O_2(b)}\left(\frac{Br_{max}}{Br_{max} - \Delta Br}\right) \tag{83}$$

Again, the substitutions for y, x, ΔBr, and β will be used as above, resulting in the following form:

$$y = x\left(\frac{Br_{max}}{Br_{max} - \Delta Br}\right) \tag{84}$$

47

$$y = x\left(\frac{1}{1 - (\Delta Br/Br_{max})}\right) \tag{85}$$

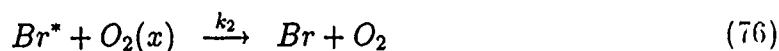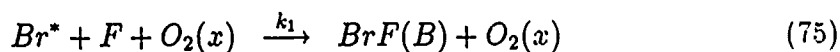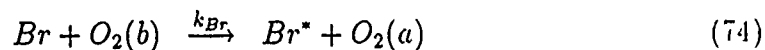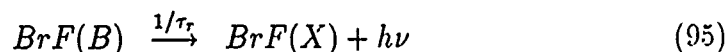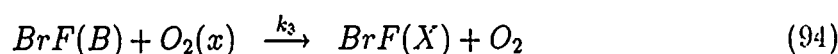$$y = x\left(\frac{1}{1 - \frac{(1-x)k_{w'}}{k_{Br}Br_{max}}}\right) \tag{86}$$

$$y = x\left(\frac{1}{1 + \frac{(x-1)\beta}{Br_{max}}}\right) \tag{87}$$

$$\frac{1}{y} = \frac{1}{x}\left(1 + \frac{(x-1)\beta}{Br_{max}}\right) \tag{88}$$

$$\frac{1}{y} = \frac{1}{x}\left(1 - \frac{\beta}{Br_{max}}\right) + \frac{\beta}{Br_{max}} \tag{89}$$

Which returns to the same form as the first variant of the 3-Body Mechanism.

The second mechanism is the 2-step excitation mechanism:

$$F + Br_2 \xrightarrow{k_1} BrF(X) + Br \tag{90}$$

$$BrF(X) + O_2(a) \xrightarrow{k_2} BrF^* + O_2(x) \tag{91}$$

$$BrF^* + O_2(b) \xrightarrow{k_p} BrF(B) + O_2(x) \tag{92}$$

$$BrF^* + O_2(x) \xrightarrow{k_q} BrF(X) + O_2 \tag{93}$$

$$BrF(B) + O_2(x) \xrightarrow{k_3} BrF(X) + O_2 \tag{94}$$

$$BrF(B) \xrightarrow{1/\tau_r} BrF(X) + h\nu \tag{95}$$
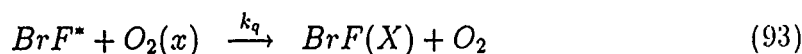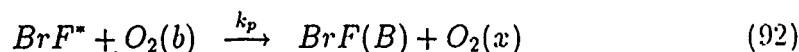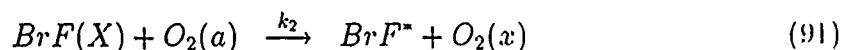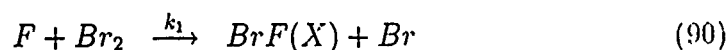
Then,

$$\frac{dBrF^*}{dt} = k_2 BrF(X)O_2(a) - k_p BrF^*O_2(b) - k_q BrF^*O_2(x) \tag{96}$$

$$\frac{dBrF(B)}{dt} = k_p BrF^*O_2(b) - k_3 BrF(B)O_2(x) - (1/\tau_r)BrF(B) \tag{97}$$

Therefore, in steady state, $dBrF^*/dt = 0$ and $dBrF(B)/dt = 0$:

$$BrF* = \frac{k_2 BrF(X) O_2(a)}{k_p O_2(b) + k_q O_2(x)} \tag{98}$$

$$BrF(B) = \frac{k_p BrF^* O_2(b)}{k_3 O_2(x) + (1/\tau_r)} \tag{99}$$

Resulting in a combined form, for both a greater amount of O atoms ($BrF(B)_o$) and a lesser amount of O atoms ($BrF(B)$), of:

$$BrF(B) = \frac{k_p k_2 O_2(a) O_2(b) BrF(X)_{max}}{(k_3 O_2(x) + (1/\tau_r))(k_p O_2(b) + k_q O_2(x))} \tag{100}$$

$$BrF(B)_o = \frac{k_p k_2 O_2(a) O_2(b)_o BrF(X)_{min}}{(k_3 O_2(x) + (1/\tau_r))(k_p O_2(b)_o + k_q O_2(x))} \tag{101}$$

Upstream of the mixing of the Br_2 and F, the Br_2 reacts with O atoms according to the following, $2(O) + Br_2 \longrightarrow 2(Br) + O_2$ (as shown before). The O atoms are removing Br_2 molecules from the flow. Resulting in an actual change in $BrF(X)$ concentration equivalent to $|\Delta BrF(X)| = |\Delta 2Br|$, and this expression will be used to substitute into the combined form of $BrF(B)$ production, both with a greater and lesser amount of O atoms, giving:

$$BrF(B) = \frac{k_p k_2 O_2(a) O_2(b)[BrF(X)_{min} + \Delta BrF(X)]}{(k_3 O_2(x) + (1/\tau_r))(k_p O_2(b) + k_q O_2(x))} \tag{102}$$

$$BrF(B)_o = \frac{k_p k_2 O_2(a) O_2(b)_o[BrF(X)_{min}]}{(k_3 O_2(x) + (1/\tau_r))(k_p O_2(b)_o + k_q O_2(x))} \tag{103}$$

$$\frac{BrF(B)_o}{BrF(B)} = \left(\frac{O_2(b)_o}{O_2(b)}\right)\left(\frac{BrF(X)_{min}}{BrF(X)_{min} + \Delta BrF(X)}\right)\left(\frac{k_p O_2(b) + k_q O_2(x)}{k_p O_2(b)_o + k_q O_2(x)}\right) \tag{104}$$

Simplifying this expression using the same substitutions for $y = BrF(B)_o/BrF(B)$, $x = O_2(b)_o/O_2(b)$, and $(\Delta Br) = (1 - x)(k_{w'}/k_{Br})$ from above, gives:

49

$$y = x\left(\frac{BrF(X)_{min}}{BrF(X)_{min} - 2(1-x)(k_{w'}/k_{Br})}\right)\left(\frac{(1/x)\left(\frac{O_2(b)_o k_p}{O_2(x)k_q}\right) + 1}{\left(\frac{O_2(b)_o k_p}{O_2(x)k_q}\right) + 1}\right) \quad (105)$$

This expression can be simplified further, putting it in the same form as the final equation for the 3 body mechanism by setting:

$$\alpha = \frac{O_2(b)_o k_p}{O_2(x)k_q} \quad (106)$$

$$\beta = \frac{k_{w'}}{k_{Br}} \quad (107)$$

$$y = x\left(\frac{BrF(X)_{min}}{BrF(X)_{min} + 2(\beta)(1-x)}\right)\left(\frac{(1/x)\alpha + 1}{\alpha + 1}\right) \quad (108)$$

$$y = x\left(\frac{1}{1 + 2(\beta)(1/BrF(X)_{min})(1-x)}\right)\left(\frac{(1/x)\alpha + 1}{\alpha + 1}\right) \quad (109)$$

Again assuming α is small, and inverting the equation:

$$y = x\left(\frac{1}{1 + (1-x)\frac{2\beta}{BrF(X)_{min}}}\right) \quad (110)$$

$$\frac{1}{y} = \frac{1}{x}\left(1 + \frac{2\beta}{BrF(X)_{min}}(1-x)\right) \quad (111)$$

$$\frac{1}{y} = \frac{1}{x}\left(1 + \frac{2\beta}{BrF(X)_{min}}\right) - \frac{2\beta}{BrF(X)_{min}} \quad (112)$$

The last equation showing clearly that the slope of the line of $1/y$ vs. $1/x$ will be greater than or equal to 1, and the intercept less than or equal to 0.

To examine which of these two processes is the primary mechanism for the pumping of BrF(B) by singlet Oxygen, an experiment will be conducted to affect the amount of O atoms in the flow tube system and the resulting emission data plotted as

described above to illustrate the behavior of the system as the amount of O atoms is changed. A branch of the O_2 inlet line will have a quantity of Mercury (Hg) placed in it so that when that branch is opened, a coating of HgO will be applied downstream of the microwave cavity and hence reduce the amount of O atoms reaching the flow tube. After this coating is applied for a set period of time, this branch will be closed and the amount of O atoms will then increase over time. Then, the line allowing only O_2 to flow will be reopened (and the O atom population will increase as the HgO coating decays). The emission of BrF(B) and O_2(b) will be recorded during both phases of the process. The emission will be recorded for sufficient time to show a significant change in the emission due to the initially decreasing and then increasing O atom population. The behavior of the plot of $\frac{I}{I_o}BrF(B)$ vs. $\frac{I}{I_o}O_2(b)$ will then show the mechanism for O_2(b) excitation of BrF(B). Due to the resultant rate equations developed in this section, this technique will provide some insight in whether the 3-Body or 2-Step Mechanisms are correct, but cannot differentiate between the two variants of the 3-Body Mechanism. See the following plot illustrating the predicted behavior.
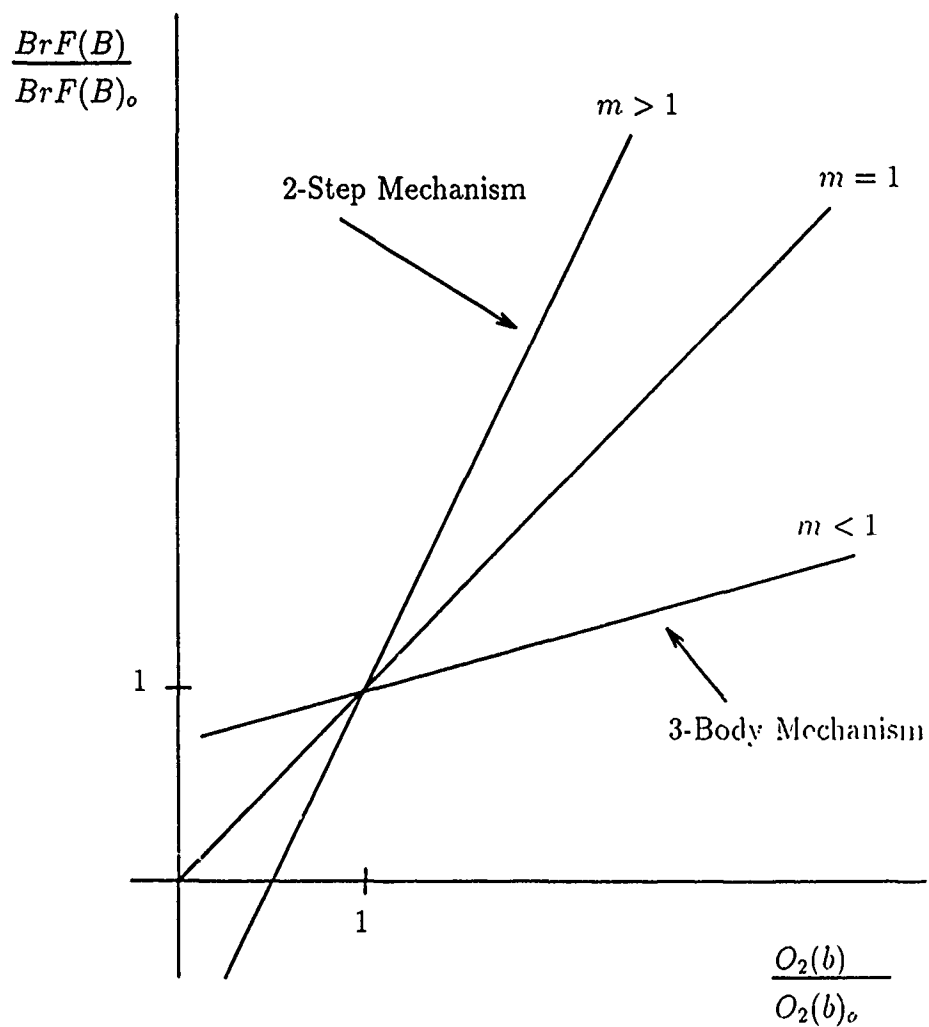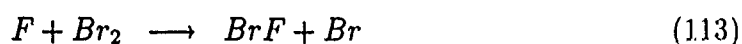
Figure 14. Plot of $\frac{I}{I_o}BrF(B)$ vs. $\frac{I}{I_o}O_2(b)$ Illustrating Relative Slopes (Theoretical) for the 3-Body and 2-Step Mechanisms

52

Appendix B. Rate Equations with CO_2 as a Quenching Species

The basic reaction in producing BrF is:

$$F + Br_2 \longrightarrow BrF + Br \tag{113}$$

This reaction is gas kinetic. In the flow tube apparatus of this experiment, this reaction essentially takes place instantaneously.

The production of singlet oxygen is determined by the following rate equations, which include the pooling reaction of $O_2(a)$, the quenching of $O_2(b)$ due to the walls (and other reagents), and the quenching of $O_2(b)$ due to CO_2:

$$O_2(a) + O_2(a) \xrightarrow{k_{pool}} O_2(b) + O_2(x) \tag{114}$$

$$O_2(b) + Wall \xrightarrow{k_w} O_2 + Wall \tag{115}$$

$$O_2(b) + CO_2 \xrightarrow{k_o} O_2 + CO_2 \tag{116}$$
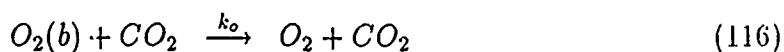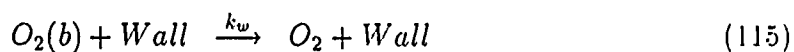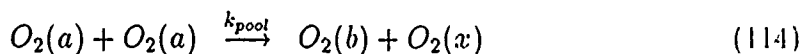
Where:

$$\frac{dO_2(b)}{dt} = k_{pool}(O_2(a))^2 - k_w O_2(b) - k_o O_2(b) CO_2 \tag{117}$$

Then, in steady state where $dO_2(b)/dt = 0$, and in the case of no CO_2 where $dO_2(b)_o/dt = 0$:

53

$$O_2(b) = \frac{k_{pool}(O_2(a))^2}{k_w + k_o CO_2} \tag{118}$$

$$O_2(b)_o = \frac{k_{pool}(O_2(a))^2}{k_w} \tag{119}$$

$$\frac{O_2(b)_o}{O_2(b)} = 1 + \frac{k_o CO_2}{k_w} \tag{120}$$

$$CO_2 = (\frac{O_2(b)_o}{O_2(b)} - 1)(\frac{k_w}{k_o}) \tag{121}$$

These results for CO_2 and O_2 will be used later.

Two primary mechanisms are considered to be responsible for the excitation of BrF(B). The first mechanism is the three body mechanism, including the effect of CO_2 within the system:

$$Br + F + O_2(x) \xrightarrow{k_1} BrF^* + O_2(x) \tag{122}$$

$$Br + F + CO_2 \xrightarrow{k_{1'}} BrF^* + CO_2 \tag{123}$$

$$BrF^* + O_2(b) \xrightarrow{k_2} BrF(B) + O_2(x) \tag{124}$$

$$BrF^* + O_2(x) \xrightarrow{k_q} BrF(X) + O_2 \tag{125}$$

$$BrF^* + CO_2 \xrightarrow{k_{q'}} BrF(X) + CO_2 \tag{126}$$

$$BrF(B) + O_2(x) \xrightarrow{k_3} BrF(X) + O_2 \tag{127}$$

$$BrF(B) + CO_2 \xrightarrow{k_{3'}} BrF(X) + CO_2 \tag{128}$$

$$BrF(B) \xrightarrow{1/\tau_r} BrF(X) + h\nu \tag{129}$$
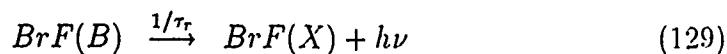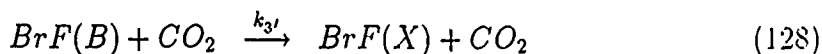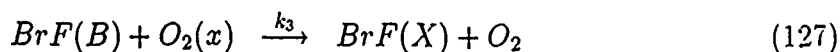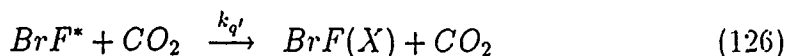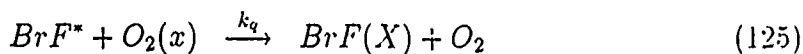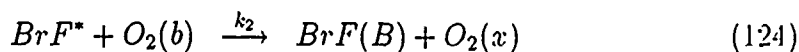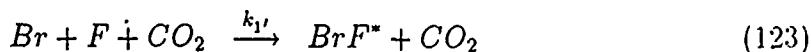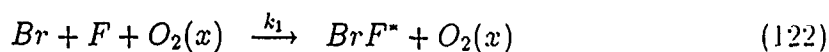
(where $O_2(x)$ is a third body, BrF^* is an excited intermediate state, and CO_2 a quenching species). Then,

$$\frac{dBrF^*}{dt} = FBr(O_2(x)k_1 + CO_2k_{1'}) - BrF^*(k_2O_2(b) + k_qO_2(x) + k_{q'}C'O_2) \quad (130)$$

$$\frac{dBrF(B)}{dt} = k_2BrF^*O_2(b) - BrF(B)(k_3O_2(x) + k_{3'}CO_2 + 1/\tau_r) \quad (131)$$

And in steady state, where $dBrF^*/dt = 0$ and $dBrF(B)/dt = 0$:

$$BrF^* = \frac{FBr(O_2(x)k_1 + CO_2k_{1'})}{k_2O_2(b) + k_qO_2(x) + k_{q'}CO_2} \quad (132)$$

$$BrF(B) = \frac{k_2BrF^*O_2(b)}{k_3O_2(x) + k_{3'}CO_2 + 1/\tau_r} \quad (133)$$

Resulting in a combined form, both with and without CO_2 present. of:

$$BrF(B) = \frac{FBrO_2(b)k_2(O_2(x)k_1 + CO_2k_{1'})}{(k_2O_2(b) + k_qO_2(x) + k_{q'}CO_2)(k_3O_2(x) + k_{3'}CO_2 + 1/\tau_r)} \quad (134)$$

$$BrF(B)_o = \frac{FBr_oO_2(x)O_2(b)_ok_1k_2}{(k_2O_2(b)_o + k_qO_2(x))(k_3O_2(x) + 1/\tau_r)} \quad (135)$$

$$\frac{BrF(B)_o}{BrF(B)} = \left(\frac{O_2(b)_o}{O_2(b)}\right)\left(\frac{k_1O_2(x)}{k_1O_2(x) + k_{1'}CO_2}\right)$$
$$\left(\frac{(k_2O_2(b) + k_qO_2(x) + k_{q'}CO_2)(k_3O_2(x) + k_{3'}CO_2 + 1/\tau_r)}{(k_2O_2(b)_o + k_qO_2(x))(k_3O_2(x) + 1/\tau_r)}\right) \quad (136)$$

$$\frac{BrF(B)_o}{BrF(B)} = \left(\frac{O_2(b)_o}{O_2(b)}\right)\left(\frac{1}{1 + \frac{k_{1'}CO_2}{k_1O_2(x)}}\right)\left(1 + \frac{k_{3'}CO_2}{k_3O_2(x) + 1/\tau_r}\right)\left(\frac{1 + \frac{k_{q'}CO_2}{k_qO_2(x)} + \frac{k_2O_2(b)}{k_qO_2(x)}}{1 + \frac{k_2O_2(b)_o}{k_qO_2(x)}}\right) \quad (137)$$

55

Simplifying this expression by using $y = BrF(B)_o/BrF(B)$, $x = O_2(b)_v/O_2(b)$, and using a substitution for $CO_2 = (x-1)(k_w/k_o)$ from above, gives:

$$y = x\left(\frac{1}{1 + \frac{k_{1'}k_w(x-1)}{k_1 k_o O_2(x)}}\right)\left(1 + \frac{k_{3'}k_w(x-1)}{k_o(k_3 O_2(x) + 1/\tau_r)}\left(\frac{1 + \frac{k_{q'}k_w(x-1)}{k_q K_o O_2(x)} + \frac{k_2 O_2(b)_o(1/x)}{k_q O_2(x)}}{1 + \frac{k_2 O_2(b)_o}{k_q O_2(x)}}\right)\right) \quad (138)$$

This expression can be simplified further by setting:

$$\alpha = \frac{k_{1'}k_w}{k_1 k_o O_2(x)} \quad (139)$$

$$\beta = \frac{O_2(b)_o k_2}{O_2(x) k_q} \quad (140)$$

$$\gamma = \frac{k_{q'}k_w}{k_q k_o O_2(x)} \quad (141)$$

$$\delta = \frac{k_{3'}k_w}{k_o(k_3 O_2(x) + 1/\tau_r)} \quad (142)$$

$$y = x\left(\frac{1}{1 + \alpha(x-1)}\right)(1 + \delta(x-1))\left(\frac{1 + \delta(x-1) + \beta(1/x)}{1 + \beta}\right) \quad (143)$$

$$y = x\frac{[(1-\delta)(1-\gamma) + \beta\delta] + [\delta(1-\gamma) + \gamma(1-\delta)]x + (\delta\gamma)x^2 + (\beta/x)(1-\delta)}{(1+\beta)((1-c) + \alpha(x))} \quad (144)$$

The second mechanism is the 2 step excitation mechanism, including reactions for CO_2 quenching:

$$F + Br_2 \xrightarrow{k_1} BrF(X) + Br \quad (145)$$

$$BrF(X) + O_2(a) \xrightarrow{k_2} BrF^* + O_2(x) \quad (146)$$

$$BrF^* + O_2(b) \xrightarrow{k_p} BrF(B) + O_2(x) \quad (147)$$

56

$$BrF^* + O_2(x) \xrightarrow{k_q} BrF(X) + O_2 \tag{148}$$

$$BrF^* + CO_2(x) \xrightarrow{k_{q'}} BrF(X) + CO_2 \tag{149}$$

$$BrF(B) + O_2(x) \xrightarrow{k_3} BrF(X) + O_2 \tag{150}$$

$$BrF(B) + CO_2(x) \xrightarrow{k_{3'}} BrF(X) + CO_2 \tag{151}$$

$$BrF(B) \xrightarrow{1/\tau_r} BrF(X) + h\nu \tag{152}$$
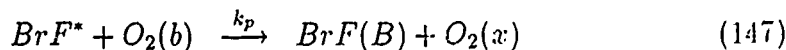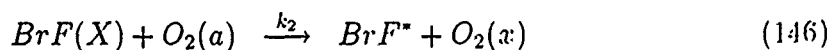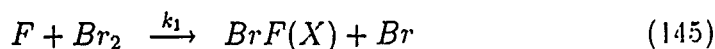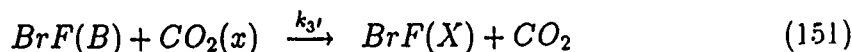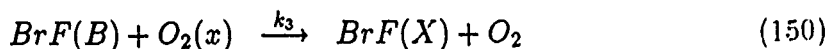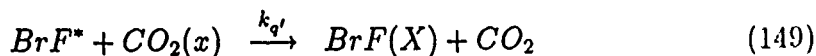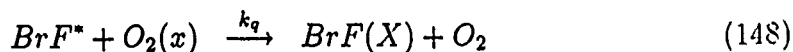
Then,

$$\frac{dBrF^*}{dt} = k_2 BrF(X)O_2(a) - BrF^*(k_p O_2(b) + k_{q'}CO_2 + k_q O_2(x)) \tag{153}$$

$$\frac{dBrF(B)}{dt} = k_p BrF^* O_2(b) - BrF(B)(k_3 O_2(x) + k_{3'}CO_2 + (1/\tau_r)) \tag{154}$$

Therefore, in steady state, $dBrF^*/dt = 0$ and $dBrF(B)/dt = 0$:

$$BrF* = \frac{k_2 BrF(X)O_2(a)}{k_p O_2(b) + k_q O_2(x) + k_{q'}CO_2} \tag{155}$$

$$BrF(B) = \frac{k_p BrF^* O_2(b)}{k_3 O_2(x) + k_{3'}CO_2 + (1/\tau_r)} \tag{156}$$

Resulting in a combined form of, both with and without CO_2 in the system:

$$BrF(B) = \frac{k_p k_2 O_2(a)O_2(b)BrF(X)}{(k_3 O_2(x) + k_{3'}CO_2 + (1/\tau_r))(k_p O_2(b) + k_q O_2(x) + k_{q'}CO_2)} \tag{157}$$

$$BrF(B)_o = \frac{k_p k_2 O_2(a)O_2(b)BrF(X)}{(k_3 O_2(x) + (1/\tau_r))(k_p O_2(b) + k_q O_2(x))} \tag{158}$$

Then, taking the ratio of the BrF(B) production terms:

57

$$\frac{BrF(B)_o}{BrF(B)} = (\frac{O_2(b)_o}{O_2(b)})$$

$$(\frac{(k_3 O_2(x) + k_{3'} CO_2 + 1/\tau_r)(k_p O_2(b) + k_q O_2(x) + k_{q'} C'O_2)}{(k_3 O_2(x) + 1/\tau_r)(k_p O_2(b)_o + k_q O_2(x))}) \quad (159)$$

Simplifying this expression using the same substitutions for $y = BrF(B)_o/BrF(B)$, $x = O_2(b)_o/O_2(b)$, and $CO_2 = (x-1)(k_w/k_o)$ from above, gives:

$$y = x(1 + \frac{k_{3'} k_w (x-1)}{k_o(k_3 O_2(x) + (1/\tau_r))})(\frac{1 + \frac{k_{q'} k_w (x-1)}{k_o k_q O_2(x)} + \frac{k_p O_2(b)_o (1/x)}{k_q O_2(x)}}{1 + \frac{k_2 O_2(b)_o}{k_q O_2(x)}}) \quad (160)$$

This expression can be simplified further, putting it in the same form as the final equation for the 3 body mechanism by setting:

$$\alpha = \frac{k_w k_{3'}}{k_o(k_3 O_2(x) + (1/\tau_r))} \quad (161)$$

$$\beta = \frac{O_2(b)_o k_2}{O_2(x) k_q} \quad (162)$$
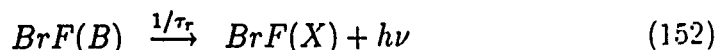
$$\gamma = \frac{k_w k_{q'}}{k_o k_q O_2(x)} \quad (163)$$

$$y = x(1 + \alpha(x-1))(\frac{1 + \gamma(x-1) + \beta(1/x)}{1 + \beta}) \quad (164)$$

$$y = \frac{x}{\beta}[\alpha\beta + (1-\alpha)(1-\gamma) + x(\gamma(1-\alpha) + \alpha(1-\gamma)) + \alpha\gamma(x^2) + (\beta/x)(1-\alpha)] \quad (165)$$

58

Appendix C. Experimental Calibrations

C.1 Spectral Response

The relative spectral response of the detection system consisting of a monochromator and a photomultiplier tube (PMT) is important in determining the relation between the observed intensity (photon counts) to the excited state relative number density. These calculations play a critical part in determining the relative vibrational population densities of the excited B-state for BrF. The relative spectral response for this experimental set-up was calculated by recording the spectrum of a blackbody source at 1000°C and comparing it to the spectrum expected from the curve generated by the Planck Blackbody Radiation Law. The emission remained in the center of the flow tube, and was resolved through the window, focusing lenses, and the 0.3 m monochromator. The number of photons detected by the PMT as a function of emission wavelength is given in Figure 15. This plot shows the normalized emission intensity for both the blackbody source and the theoretical Planck blackbody radiation distribution, as well as the normalized relative spectral response. The relative spectral response itself ($D(\nu)$) is calculated from (28):

$$D(\nu) = n_d(\nu)/n_{bb}(\nu) \tag{166}$$

where:

$n_d(\nu)$ =the number of photons/sec detected by the PMT

$n_{bb}(\nu)$ =the number of photons/sec emitted by an ideal blackbody

A listing of the relative spectral responses for the observed emission transitions for BrF are shown in Table 10. All values for the spectral response have been normalized to the maximum value at 6700 Å from Figure 15.

Table 10. Relative Spectral Response

Transition (v',v'')	Wavelength (in Å)	Franck-Condon Factor $q_{v',v''}$	Spectral Response $D(\nu)$
(6,3)	5496	0.0256	0.4000
(5,3)	5586	0.0489	0.4500
(5,7)	6510	0.0222	0.9000
(4,3)	5686	0.0682	0.5100
(4,6)	6390	0.0288	0.8200
(4,7)	6648	0.0526	0.9750
(4,8)	6928	0.0180	0.9370
(4,10)	7550	0.0410	0.7200
(3,3)	5796	0.0738	0.6000
(3,4)	6033	0.0671	0.7000
(3,5)	6270	0.0205	0.8390
(3,7)	6800	0.0392	0.9671
(3,8)	7090	0.0625	0.8870
(3,9)	7406	0.0274	0.7950
(2,3)	5916	0.6000	0.6800
(2,4)	6160	0.0875	0.7800
(2,5)	6410	0.0723	0.8350
(2,6)	6679	0.0235	0.9850
(2,8)	7266	0.0334	0.8550
(1,3)	6054	0.0345	0.7200
(1,4)	6300	0.0726	0.8439
(1,5)	6560	0.1044	0.9250
(1,6)	6840	0.1012	0.9550
(1,7)	7138	0.0589	0.8820
(1,8)	7462	0.0113	0.7700
(0,4)	6448	0.0296	0.8600
(0,5)	6723	0.0635	0.9800
(0,6)	7012	0.1073	0.9300
(0,7)	7330	0.1480	0.8200
(0,8)	7676	0.1675	0.6650

60
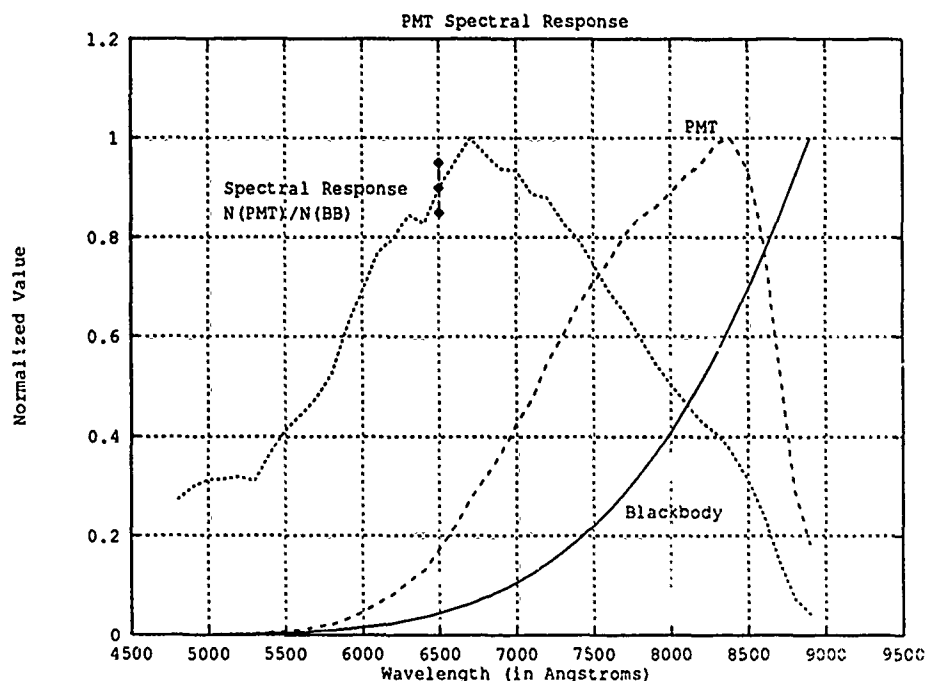
Figure 15. Spectral Response of C31034 PMT with Blackbody at 1000°C

C.2 Monochromator Calibration

The resolution of the 0.3m monochromator is shown in Figure 16. Melton determined this resolution, as a function of slit width using a Neon flashlamp prior to my involvement with the research (26). A linear least squares fir of the data returned a nearly linear relationship with $corr^2 = 99.15\%$. Extrapolating this result for slits with a width of 300μm, a 7Å (0.7nm) resolution was obtained. Using 300μm slits. sufficient signal strengths as well as favorable signal-to-noise ratios were obtained for all the BrF(B) ⟶ BrF(X) vibrational transitions with $5800Å \leq \lambda < 7800Å$ as listed in Clyne and Coxon (5). Even though the 300μm slits were not small enough to clearly resolve the closely lying vibrational transitions at $\lambda < 5800.Å$, the structure was observed and could be estimated given the known values for these transitions as shown in Clyne and Coxon (5).

Melton determined the absolute wavelength of the 0.3m monochromator using

61
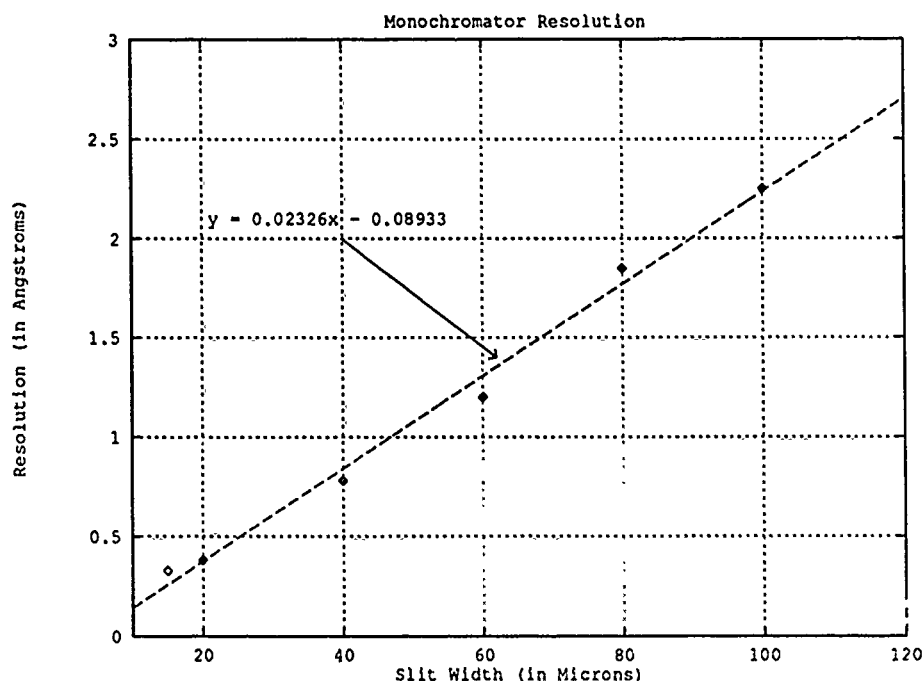
Figure 16. Monochromator Resolution with Least Squares Fit Resultant

a Neon discharge lamp previously(26). Over the range of interest. $5000\overset{\circ}{A} < \lambda < 7800\overset{\circ}{A}$, the calibration correction was an average of $6.4\overset{\circ}{A}$, with a standard deviation of $0.3\overset{\circ}{A}$. Since the monochromator was calibrated only to the nearest Angstrom. a value of $6\overset{\circ}{A}$ was therefore used as the wavelength correction.

Table 11. Wavelength Calibration of 0.3 m Monochromator

Monochromator $\lambda(\overset{\circ}{A})$	7482.0	6923.5	6592.5	6024.1	5846.0	5394.2
Actual $\lambda(\overset{\circ}{A})$	7488.9	6929.9	6599.0	6030.0	5852.5	5400.6
Difference $\lambda(\overset{\circ}{A})$	0006.9	0006.4	0006.5	0005.9	0006.5	0006.4

C.3 Metering Valve Calibration

The Nupro metering valves were calibrated by connecting a Kontes valve between the flow tube and the cold trap so that the exhaust could be closed and the time rate of change of the pressure (dP/dt) in the flow tube be measured. First. the leak rate was measured and then dP/dt for the different valve settings of the

CF_4 and Br_2 inlets were measured. The flow tube set-up as configured in Figure 5 was determined to have a leak rate of 0.173 $torr/min$ and this value was subtracted from the values recorded for the different CF_4 and Br_2 valve settings to give dP/dt for the CF_4 and Br_2 inlets, respectively. The total volume of the system forward of the valves was measured to be $Volume = 3276 \ cm^3$. Once dP/dt was for each valve was recorded, the actual dP/dt and dn/dt (in sccm) were obtained from:

$$\frac{dP_{actual}}{dt} = \frac{dP_{recorded}}{dt} - 0.173\frac{torr}{min} \tag{167}$$

$$\frac{dn}{dt} = (\frac{dP_{actual}}{dt})(\frac{3276cm^3}{760torr}) \tag{168}$$

For the two different CF_4 valve settings of 2.0 and 2.2 revolutions, the following values of dn/dt were obtained:

dn/dt @2.2 revolutions = 190.4 sccm

dn/dt @2.0 revolutions = 184.15 sccm

For the many varying settings of the Br_2 valve, the values of dn/dt obtained are listed in Table 12.

No values for valve settings less than 0.8 revolution were used since dP/dt was unchanged and no observable effect seen on the output signal. The value of dn/dt for valve set at 1.0 revolution was interpolated linearly between the values at 0.8 and 1.2 revolutions because although no dP/dt was observed different from 0.8 revolutions, there was a noticeable effect on the output signal; specifically, significant reduction in the $O_2(^1\Sigma)$ emission was observed (quenching).

Once BrF was actually produced (Section 3.1), the number density for Br_2 could be calculated. Given constant inputs for $O_2(x)$ at 848 sccm and CF_4 at either 190.4 or 184.15 sccm, first the partial pressure of Br_2 was determined and then the number density of Br_2 calculated from the following:

Table 12. dn/dt for Br_2 Valve Settings

Set (# revs)	dn/dt (sccm)
0.0	0.0000
0.8	0.0776
1.0	0.0862
1.2	0.0948
1.4	0.1035
1.6	0.1121
1.8	0.1897
2.0	0.2414
2.2	0.2974
2.4	0.3664
2.6	0.4397
2.8	0.5776
3.0	0.6509
4.0	1.2113
5.0	1.8449

$$P_{Br_2} = (\frac{\dot{n}(Br_2)}{\dot{n}(Br_2) + \dot{n}(CF_4) + \dot{n}(O_2)})P_{total} \qquad (169)$$

$$n = (\frac{P_{Br_2}}{760 torr})(2.6868 \times 10^{19} cm^{-3})(\frac{273K}{300K}) \qquad (170)$$

where:

$\dot{n} \equiv$ dn/dt

Loschmidt's Number (at STP) $= 2.6868 \times 10^{19} cm^{-3}$

The calculated values for the Br_2 number density (for the two different flow rates of CF_4), at the different valve settings are listed in Table 13.

C.4 Other Considerations

This section will list some of the other considerations that affected the system. especially as they influenced BrF and O_2(b) production.

Table 13. Br_2 Number Density at Varying Valve Settings

Set (# revs)	n (cm^{-3}) (@CF_4 = 190.4 sccm)	n (cm^{-3}) (@CF_4 = 184.15 sccm)
0.0	0.0000	0.0000
0.8	8.3646x10^{12}	8.0984x10^{12}
1.0	9.2940x10^{12}	8.9982x10^{12}
1.2	1.0223x10^{13}	9.8979x10^{12}
1.4	1.1153x10^{13}	1.0798x10^{13}
1.6	1.2082x10^{13}	1.1697x10^{13}
1.8	2.0445x10^{13}	1.9794x10^{13}
2.0	2.6019x10^{13}	2.5191x10^{13}
2.2	3.2058x10^{13}	3.1037x10^{13}
2.4	3.9489x10^{13}	3.8232x10^{13}
2.6	4.7383x10^{13}	4.5875x10^{13}
2.8	6.2240x10^{13}	6.0259x10^{13}
3.0	7.0131x10^{13}	6.7899x10^{13}
4.0	1.3044x10^{14}	1.2629x10^{14}
5.0	1.9855x10^{14}	1.9223x10^{14}

1. If the system was opened to air for a short period of time, such as to change the cold trap, about 15 to 30 minutes were needed to pump the system back down to its optimum pressure ($\sim$ 100 millitorr), as well as get rid of the ambient air in the system.

2. If the system was opened to air for a long period of time, such as after the valve calibration study, the system had to be pumped down for an extended time (anywhere from 1 hour to a full day) to reduce outgassing, the effect of H_2O vapor build-up in the system, and return the system to its optimum pressure.

3. The wall rate was noted to change on a daily basis. Therefore, all experiments conducted included determining the wall rate for that particular experiment. This wall rate was then used in the calculations to determine the other rate constants.

4. It was noted that microwave discharge efficiency had an effect on the system. Either due to the age (or operating characteristics) of the Opthos Microwave Cavities, or the effect of the daily changes in the system, the desired reduction of reflected power to a minimum was not a constant. Generally, the forward to reflected power ratio for the O_2 microwave cavity was 100/2, with the reflected power varying from 0 to 4. This affected the amount of $O_2(b)$ produced by approximately 50% (for the worst case). Fortunately, keeping track of the daily $O_2(b)$ production allowed the experments to be run when the efficiency was good. Interestingly, a similar effect was not noted with the microwave cavity dissociating CF_4, even when the cavities were switched.

Appendix D. Vibrational Population Calculations

D.1 Calculations

The following tables outline the actual calculations used in determining the vibrational populations of the v-states of BrF(B). The transition listed in this section were the clearly resolvable transitions recorded on the emission spectrum for BrF(B). The basic formulas used as listed in the main text are repeated here.

$$I^{emm} = I^{obs}/D$$

$$Pop(BrF(B)_v) = (\frac{I^{emm}_{BrF(B)_v}(\tau_r)}{I^{emm}_{O_2(b)}(\tau_{rO_2(b)})})Pop(O_2(b))$$

The resulting values for $Pop(BrF(B)_v)$ are recorded under the heading $N_{v',v''}$ in the tables below.

Transitions originating at v'= 0

v'→v"	τ_r (μsec)	FCF	Population $N_{v',v''}$
0-4	43.0	.0296	1.66×10^7
0-5		.0635	7.16×10^7
0-6		.1073	1.09×10^8
0-7		.1480	1.48×10^8
0-8		.1657	1.38×10^8
Total		.5141	4.83×10^8

v'→v"	τ_r (μsec)	FCF	Population $N_{v',v''}$
1-3	44.0	.0345	4.07×10^7
1-4		.0726	1.65×10^8
1-5		.1044	2.66×10^8
1-6		.1012	2.15×10^8
1-7		.0589	1.31×10^8
1-8		.0113	4.38×10^7
Total		.3829	8.62×10^8

Transitions originating at v'= 1

v'→v"	τ_r (μsec)	FCF	Population $N_{v',v''}$
2-3	46.0	.0600	4.21×10^8
2-4		.0875	3.77×10^8
2-5		.0723	3.21×10^8
2-6		.0235	9.64×10^7
2-8		.0334	1.61×10^7
Total		.2767	12.32×10^8

Transitions originating at v'= 2

v'→v"	τ_r (μsec)	FCF	Population $N_{v',v''}$
3-3	43.9	.0738	4.60×10^8
3-4		.0671	3.57×10^8
3-5		.0205	1.45×10^8
3-7		.0392	3.32×10^7
3-8		.0625	8.90×10^7
3-9		.0274	4.41×10^7
Total		.2905	11.28×10^8

Transitions originating at v'= 3

68

Transitions originating at v'= 4

v'→v"	τ_r (μsec)	FCF	Population $N_{v',v''}$
4-3	44.7	.0682	4.97×10^8
4-6		.0288	3.63×10^7
4-7		.0520	7.17×10^7
4-8		.0180	3.33×10^7
4-10		.0410	1.86×10^7
Total		.2080	6.57×10^8

Transition originating at v'= 5

v'→v"	τ_r (μsec)	FCF	Population $N_{v',v''}$
5-7	44.2	.0222	3.43×10^7

69

D.2 Detailed Emission Spectra

This section includes reproductions of the detailed emission spectra taken with $300\mu m$ slits, but at a much slower scan speed than the global spectrum illustrated in the main body of the text. Here, the experimental settings were:

- $300\mu m$ slits

- $20 Angstrom/min$ monochromator scan

- $1cm/min$ paper speed

- Resulting in a recorded measurement of $20 Angstrom/cm$ on the strip chart

- $0.4sec$ photon counter integration time

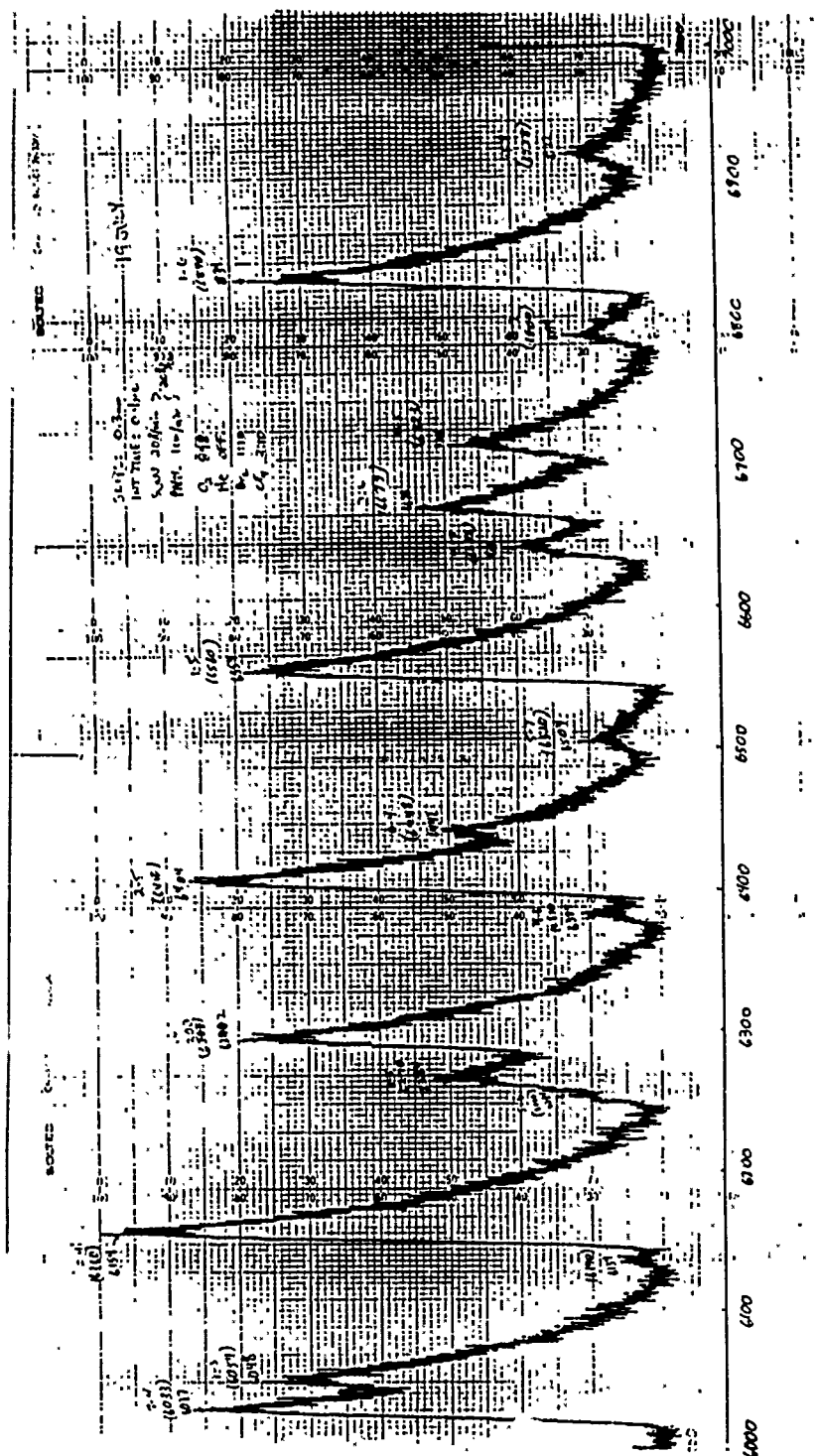Figure 17. Detailed Emission Spectrum of BrF(B) Part 1
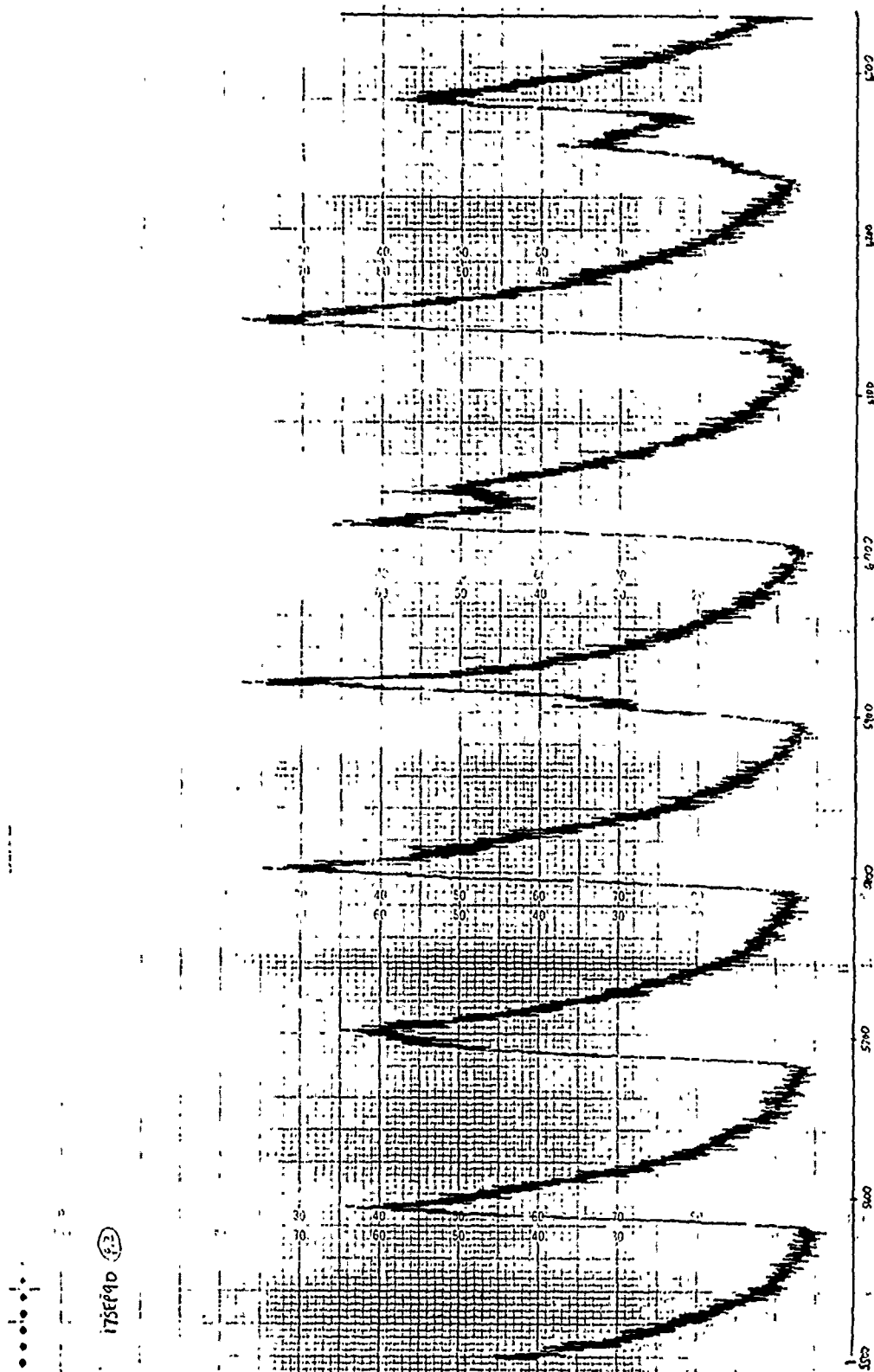
71

Figure 18. Detailed Emission Spectrum of BrF(B) Part 2

72

Figure 19. Detailed Emission Spectrum of BrF(B) Part 3

Appendix E. Photograph of BrF(B) Emission

Output Window   Flow Tube

Shape of
Emission

O₂ Flow   (850 sccm)

Br₂ Inlet (0.19 sccm)

O₂ Flow
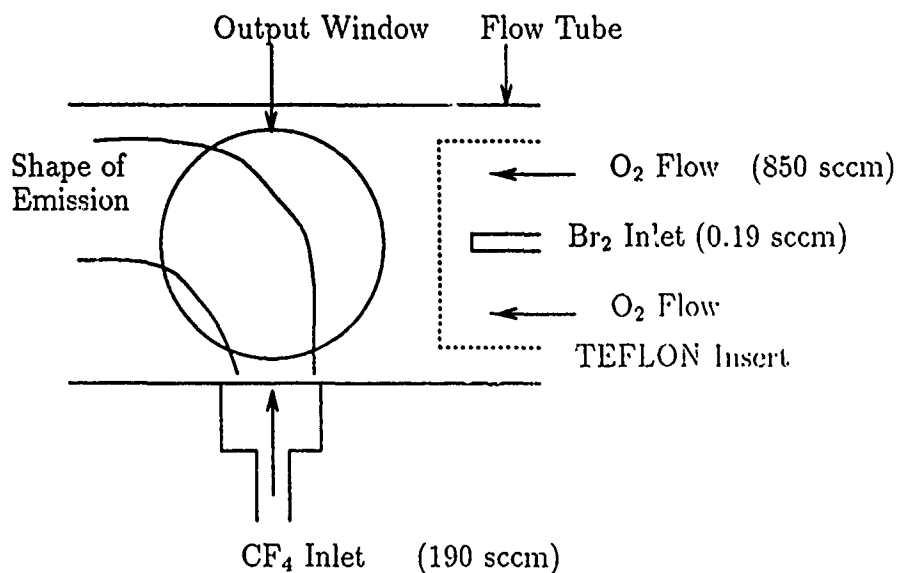
TEFLON Insert

CF₄ Inlet   (190 sccm)

Figure 20. Schematic of BrF(B) Emission

A photograph of the actual BrF(B) emission is shown on the next page. This picture was taken with ASA 1600 color film with a 60 second exposure time.
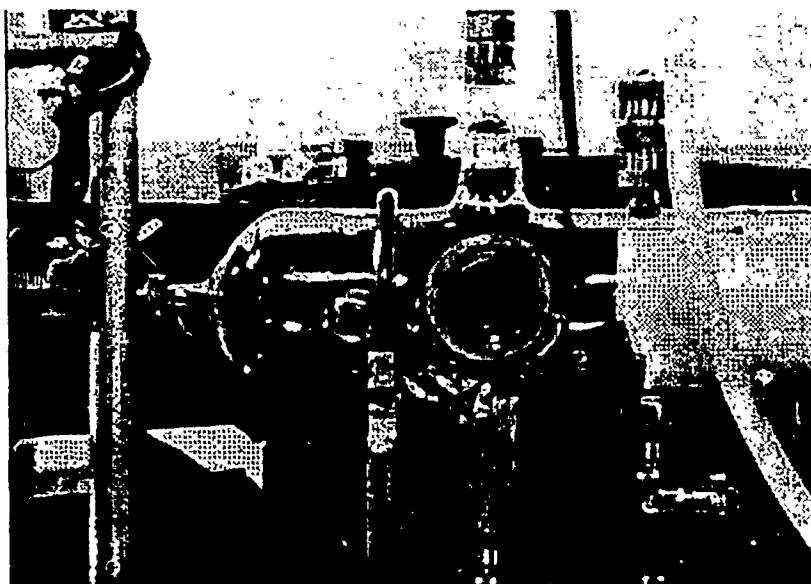
Figure 21. Photograph of BrF(B) Emission

Bibliography

1. Perram, G. P. , "Visible Chemical Lasers", Proceedings from the International Conference on LASERS '89, (Preprint), (1989).

2. Davis, S. J. , "Prospects for Visible Chemical lasers", SPIE Vol 540, Southwest Conference on Optics (1985), pp188-195.

3. Davis, S. J. , L. Hanko, and P. J. Wolf, "Continuous wave optically pumped iodine monofluoride $B^3\Pi(0^+) \longrightarrow X^1\Sigma^+$ laser", *Journal of Chemical Physics*. *82*, (1985), p4831.

4. Melton, D. W. , "Collisional dynamics of the $B^3\Pi(0^+)$ state of bromine monofluoride", AFIT DS-91 Prospectus, (Unpublished), (1990).

5. Clyne, M. A. A. , J. A. Coxon, and L. W. Townsend, "Formation of the $B^3\Pi(0^+)$ states of BrF and IF by atom recombination in the presence of singlet ($^1\Delta_g$, $^1\Sigma_g^+$) oxygen", *Journal of the Chemical Society Faraday II, 68*, (1972), p2134.

6. Howard, C. J. , "Kinetic measurements using flow tubes", *Journal of Physical Chemistry, 83*, (1979), p3.

7. Davis, S. , "Potential of Halogen Molecules as Visible Chemical Laser Systems". AFWL-TR-79-104, (1979), p167.

8. Clyne, M. A. A. , and I. S. McDermid, "Stable Levels of the $B^3\Pi(0^+)$ State of BrF", *Journal of the Chemical Society Faraday II, 74*, (1978). p664.

9. Coxon, J. A. , and A. H. Curran, "High Resolution Analysis of the $B^3\Pi(0^+) \longleftarrow X^1\Sigma^+$ Transition of BrF", *Journal of Molecular Spectroscopy, 75*, (1979), p270.

10. Durie, R. A. , "The Visible Spectra of Iodine and Bromine Monofluorides and their Dissociation Energies", *Proceedings of the Royal Society A. 207*, (1951). p288.

11. Clyne, M. A. A. , A. H. Curran, and J. A. Coxon, "Studies of Labile Molecules with a Tunable Dye Laser", *Journal of Molecular Spectroscopy. 63*. (1976), p13.

12. Steinfeld, J. , "Rate Data for Inelastic Collision Processes in Diatomic Halogens", *Journal of Physical and Chemical Reference Data, 13*, (1984), p.445.

13. Perram, G. P. , "Energy transfer from singlet oxygen to bromine monofluoride: Thesis problem statement and background information", GEP-90D, AFIT, (Unpublished), (1989).

14. Setser, D. W. , *Reactive Intermediates in the Gas Phase*, New York: Academic Press, (1979).

15. Plummer, D. N. , R. F. Heider, and G. Perram, *Proceedings from the 1987 Conference on COIL Kinetics*, Albuquerque: RDA Associates. (1988).

16. Ranby, B. and J. F. Rabek, *Singlet Oxygen*, New York: John Wiley and Sons. Inc. , (1979).

17. Davidson, J. and E. Ogryzlo, "The Quenching of Singlet Molecular Oxygen", *Chemiluminescence and Bioluminescence*, edited by M. J. Cormier, et al. , New York: Plenum Press, (1977).

18. Singh, J. P. , et al. , "Electronic to Vibrational Energy Transfer Studies of Singlet Oxygen; 1. $O_2(a^1\Delta_g)$", *Journal of Physical Chemistry, 89*, (1985), p5347.

19. Singh, J. P. et al. , "Electronic to Vibrational Energy Transfer Studies of Singlet Oxygen; 2. $O_2(b^1\Sigma_g^+)$", *Journal of Physical Chemistry, 89*, (1985), p5353.

20. Mack, R. T. , "Singlet Oxygen and Iodine Monofluoride Collisional Energy Transfer Mechanism", AFIT GEP-89D, Master's Thesis, (Unpublished), (1989).

21. Brodersen, P. , and J. Sicre, "Das Spektrum des BrF und seine Dissoziationsenergie", *Zeitschrift für Physik, Band 141*, (1955), p514.

22. Coxon, J. A. , "Dissociation Energies of Diatomic Halogen Fluorides". *Chemical Physics Letters, 33*, (1975), p136.

23. Donovan, R. , and D. Husain, "Chemistry of Electronically Excited Atoms". *Chemical Reviews, 70*, (1970), p509.

24. Davis, S. , et al. , *Excitation of IF($B^3\Pi(0^+)$) by Singlet Oxygen: Energy Transfer from $O_2(^1\Sigma)$*, PSI-2000/SR-364, Andover, Md: Physical Sciences. Inc. , (1989).

25. Davis, S. , et al. , *Excitation of IF($B^3\Pi(O^+)$) by Metastable O_2. Studies Involving IF(X,v)*, PSI-2000/SR-395, Andover, Md: Physical Sciences. Inc. , (1989).

26. Melton, D. W. , Doctoral Student, Department of Physics, Air Force Institute of Technology, personal discussions at AFIT, April - September 1990.

27. Kolb, C. E. , and M. Kaufman, "Molecular Beam Analysis Investigation of the Reaction between Atomic Fluorine and Carbon Tetrachloride". *Journal of Physical Chemistry, 76*, (1972), p947.

28. Perram, Glen P. , "Collisional Dynamics of the $B^3\Pi(O^+)$ State of Bromine Monochloride", Dissertation, AFIT DS-86, (1986).

77

Vita

CPT Barrett F. Lowe was born on 21 February 1959 in Alexandria, Virginia. After graduating from Frank W. Cox High School in Virginia Beach, Virginia in 1977, he was accepted into the Corps of Cadets at the United States Military Academy at West Point. He graduated from West Point with a B.S. in Engineering in 1981 and was commissioned in the Infantry. He attended the Infantry Officer Basic Course and Ranger School at Fort Benning, Georgia in 1981. His first assignment was to the 1st Battalion (Airborne) 509th Infantry in Vicenza, Italy, where he served as a Rifle Platoon Leader, Mortar Platoon Leader, and a Battalion Staff Officer from 1982 to 1985. Returning to the Continental United States, he attended the Infantry Officer Advanced Course at Fort Benning prior to his second assignment, which was to the 101st Airborne Division (Air Assault) at Fort Campbell, Kentucky. He served as the Battalion S-3 Air Staff Officer in the 3rd Battalion 327th Infantry in 1985 and early 1986. He was then selected by the Division Commander to activate and command the Division Long Range Surveillance Detachment (LRSD) in the 2nd Squadron 17th Cavalry. He left command of the LRSD in 1987 and returned to the 3rd Battalion 327th Infantry to assume command of C Company. He remained in command until early 1989 when he received orders to attend graduate school at the Air Force Institute of Technology. Upon completion of his degree, he will join the staff and faculty at West Point as an Instructor in the Department of Physics.

CPT Lowe's awards and decorations include the Meritorious Service Medal, the Army Commendation Medal (with Oak Leaf Cluster), the Ranger Tab, the Expert Infantryman's Badge, the Master Parachutist's Badge, the Pathfinder Badge, the Air Assault Badge, and the German Army Parachutist's Badge.

He is married to the former Elizabeth Anne Parry, of Minneapolis, Minnesota. Their son, James Barrett (Jeb), was born on 16 October 1986 at Fort Campbell. Kentucky.

Permanent address: 1497 Wakefield Drive
Virginia Beach, Virginia
23455

REPORT DOCUMENTATION PAGE

1. AGENCY USE ONLY (Leave blank)	2. REPORT DATE	3. REPORT TYPE AND DATES COVERED
	December 1990	

4. TITLE AND SUBTITLE

ENERGY TRANSFER IN SINGLET OXYGEN AND BROMINE MONOFLUORIDE

5. FUNDING NUMBERS

6. AUTHOR(S)

Barrett F. Lowe, CPT, US Army

7. PERFORMING ORGANIZATION NAME(S) AND ADDRESS(ES)

Air Force Institute of Technology, WPAFB, OH 45433-6583

8. PERFORMING ORGANIZATION REPORT NUMBER

AFIT/GEP/ENP/90D-2

9. SPONSORING / MONITORING AGENCY NAME(S) AND ADDRESS(ES)

10. SPONSORING / MONITORING AGENCY REPORT NUMBER

11. SUPPLEMENTARY NOTES

12a. DISTRIBUTION / AVAILABILITY STATEMENT

Approved for public release; distribution unlimited.

12b. DISTRIBUTION CODE

13. ABSTRACT (Maximum 200 words)

The interhalogen molecule, bromine monofluoride (BrF), is currently under study as a potential candidate for a visible chemical laser medium. Previous studies have shown a strong emission from BrF(B) in the presence of singlet oxygen, O_2(b) and O_2(a). While singlet oxygen will pump BrF(X) to BrF(B), the exact mechanism is not known. Chemiluminescence observed from BrF(B) excited by O_2(b) in a gas flowtube was used to study the energy transfer mechanism. The objective of this research was fourfold. First, the pumping process was identified as a 3-Body Mechanism. Second, the observed vibrational distribution clearly showed the population of the BrF(B) state to be non-Maxwellian. Third, the quenching rates for CO_2 and CF_4 on O_2(b) were experimentally verified with the literature values, and the quenching rates for Br and Br_2 on O_2(b) are reported for the first time. And fourth, the efficiency of the system is shown to be low, on the order of 10^{-4}.

14. SUBJECT TERMS

Chemical Lasers, Visible Chemical Lasers, Spectroscopy, Lasers, Bromine Monofluoride, Bromine, Singlet Oxygen

15. NUMBER OF PAGES

88

16. PRICE CODE

17. SECURITY CLASSIFICATION OF REPORT	18. SECURITY CLASSIFICATION OF THIS PAGE	19. SECURITY CLASSIFICATION OF ABSTRACT	20. LIMITATION OF ABSTRACT
Unclassified	Unclassified	Unclassified	UL